



# Geochemical provenance of sediments from the northern East China Sea document a gradual migration of the Asian Monsoon belt over the past 400,000 years

François Beny <sup>a,b,c,\*</sup>, Samuel Toucanne <sup>a</sup>, Charlotte Skonieczny <sup>a,d</sup>, Germain Bayon <sup>a</sup>, Martin Ziegler <sup>e</sup>

<sup>a</sup> IFREMER, Laboratoire Géodynamique et Enregistrement Sédimentaire, ZI de La Pointe Du Diable, CS 10070, 29280 Plouzané, France

<sup>b</sup> Univ. Lille, CNRS, Univ. Littoral Côte D'Opale, UMR 8187, LOG, Laboratoire D'Océanologie et de Géosciences, F 59000 Lille, France

<sup>c</sup> VU University Amsterdam, Department of Earth Sciences, Faculty of Science, De Boelelaan 1085, 1081 HV Amsterdam, The Netherlands

<sup>d</sup> Laboratoire GEOsciences Paris-Sud (GEOPS), UMR CNRS 8148, Université de Paris-Sud, Université Paris-Saclay, 91405 Orsay Cedex, France

<sup>e</sup> Utrecht University, Heidelberglaan 2 3584CS Utrecht, The Netherlands



## ARTICLE INFO

### Article history:

Received 2 November 2017

Received in revised form

25 April 2018

Accepted 29 April 2018

Available online 9 May 2018

### Keywords:

Monsoon

Eastern Asia

East China sea

Quaternary

Radiogenic isotopes

Neodymium

Rare earth elements

## ABSTRACT

The reconstruction of the long-term evolution of the East Asian Monsoon remains controversial. In this study, we aim to give a new outlook on this evolution by studying a 400 kyr long sediment record (U1429) from the northern East China Sea recovered during IODP Expedition 346. Neodymium isotopic ratios and rare earth element concentrations of different grain-size fractions reveal significant provenance changes of the sediments in the East China Sea between East Asian continental sources (mainly Yellow River) and sediment contributions from the Japanese Archipelago. These provenance changes are interpreted as the direct impact of sea level changes, due to the reorganization of East Asian river mouth locations and ocean circulation on the East China Sea shelf, and latitudinal shifts of the intertropical convergence zone (ITCZ) from the interior of Asia to the western North Pacific Ocean. Our data reveal the dominance of winter and summer monsoons during glacial and interglacial periods, respectively, except for glacial MIS 6d (~150–180 ka) during which unexpected summer monsoon dominated conditions prevailed. Finally, our data suggests a possible strengthening of the interglacial summer monsoon rainfalls over the East Asian continent and Japan throughout the past 400 kyr, and between MIS 11 and MIS 5 in particular. This could result from a gradual northward migration of the ITCZ.

© 2018 Elsevier Ltd. All rights reserved.

## 1. Introduction

The distribution of rainfall associated with the global monsoon system is tightly linked to the seasonal latitudinal shifts of the intertropical convergence zone (ITCZ), with high precipitation occurring in East Asia during the boreal summer when the ITCZ is located in the northern hemisphere. Our understanding of past East Asian monsoon dynamics is mainly based on reconstructions from continental archives such as speleothems (Wang et al., 2001, 2008; Yuan et al., 2004; Dykoski et al., 2005; Jo et al., 2014; Cheng et al., 2016), loess sequences (Zhisheng et al., 2001; Sun et al., 2006; Yang and Ding, 2008; Meng et al., 2018) and lacustrine sedimentary

records (An et al., 2000; Xiao et al., 2004). These studies provide substantial information on the evolution of the East Asian Monsoon system during the Pleistocene, documenting paleoclimatic records exhibiting glacial-interglacial (loess records) and/or precessional cyclicity (speleothems).

Marine sediments deposited in the East China Sea, in addition to South China Sea sedimentary records (e.g. Wang et al., 1999; Liu et al., 2003), represent suitable archives for investigating the evolution of the East Asian monsoon over glacial-interglacial timescales (e.g. Chang et al., 2009). The East China Sea serves as a sink for the particulate load delivered by the Yangtze (Changjiang) and Yellow (Huanghe) rivers systems, two of the world's longest rivers. Their drainage areas are strongly influenced by monsoon-dominated climate. Sedimentary archives from the Yangtze and Yellow rivers deltas (Yi et al., 2003; Yi and Saito, 2004; Chen et al., 2005a,b; Xiao et al., 2006), as well as from the Okinawa Trough in

\* Corresponding author. IFREMER, Laboratoire Géodynamique et enregistrement Sédimentaire, ZI de la Pointe du Diable, CS 10070, 29280 Plouzané, France.  
E-mail address: [francois.beny@univ-lille1.fr](mailto:francois.beny@univ-lille1.fr) (F. Beny).

the northern East China Sea (Sun et al., 2005; Yu et al., 2009; Kubota et al., 2010; Zhao et al., 2018), have been used to reconstruct the East Asian Monsoon signal back to the last glacial maximum ~20–30 ka. In these studies, the evolution of the East Asian monsoon was reconstructed from the flux of East Asian river detrital sediments to nearby oceanic areas (Saito et al., 2001; Liu et al., 2007; Hu et al., 2012). In particular, these fluxes were inferred through the tracking of the chemical and mineralogical signatures of Yangtze and/or Yellow rivers sediments as far as the Okinawa Trough (Diekmann et al., 2008; Dou et al., 2010, 2012; Xu et al., 2014; Li et al., 2015; Zhao et al., 2017, 2018). However, there are a lack of sedimentary archives recording the response of East Asian river basins to monsoon-related climatic changes over several interglacial-glacial cycles. Such records are necessary to understand the long-term variability of East Asian monsoon and its response to orbital forcing. In this study, we aim at filling this gap by studying a marine sediment record (U1429; Fig. 1) covering the last 400 kyr and recovered in the northern Okinawa Trough during the Integrated Ocean Drilling Program (IODP) Expedition 346 (Expedition 346 Scientists, 2014). The approach developed in this study is based on a detailed geochemical investigation of the detrital fraction of the U1429 Site sediments by combining major and rare earth element (REE) concentrations and neodymium (Nd) isotopic ratios. These proxies provide valuable information on

sediment provenance. In the context of monsoon-dominated climates, these proxies allow us to reconstruct the response of river systems to past hydroclimate changes. Because decoupling of REE and Nd isotopes may occur between different grain-size fractions during hydrodynamic sorting and weathering processes, with possible implications for their use as provenance proxies (e.g. Meyer et al., 2011; Garçon and Chauvel, 2014; Bayon et al., 2015), we analyse several targeted grain-size fractions.

## 2. The East Asian sediment-routing systems

### 2.1. Geography, geology and climatology of the East Asian drainage systems

The Yangtze River (6400 km in length; drainage area of  $1807 \times 10^3 \text{ km}^2$ ) and the Yellow River (5450 km in length; drainage area of  $752 \times 10^3 \text{ km}^2$ ) are the two major drainage systems in East Asia (Fig. 1). Both rivers start in the northeast Tibetan Plateau (Qinghai Province) at about 5000 m elevation and flow eastward, delivering a total sediment flux of about  $1,600 \times 10^6 \text{ t/yr}$  to the East China Sea (Milliman and Syvitski, 1992; Saito et al., 2001). Although a significant part of this flux (~60%) is derived from the Yellow river, the Chinese Loess Plateau in particular, the Yangtze river was likely the main source of sediment to the East China Sea prior to the onset

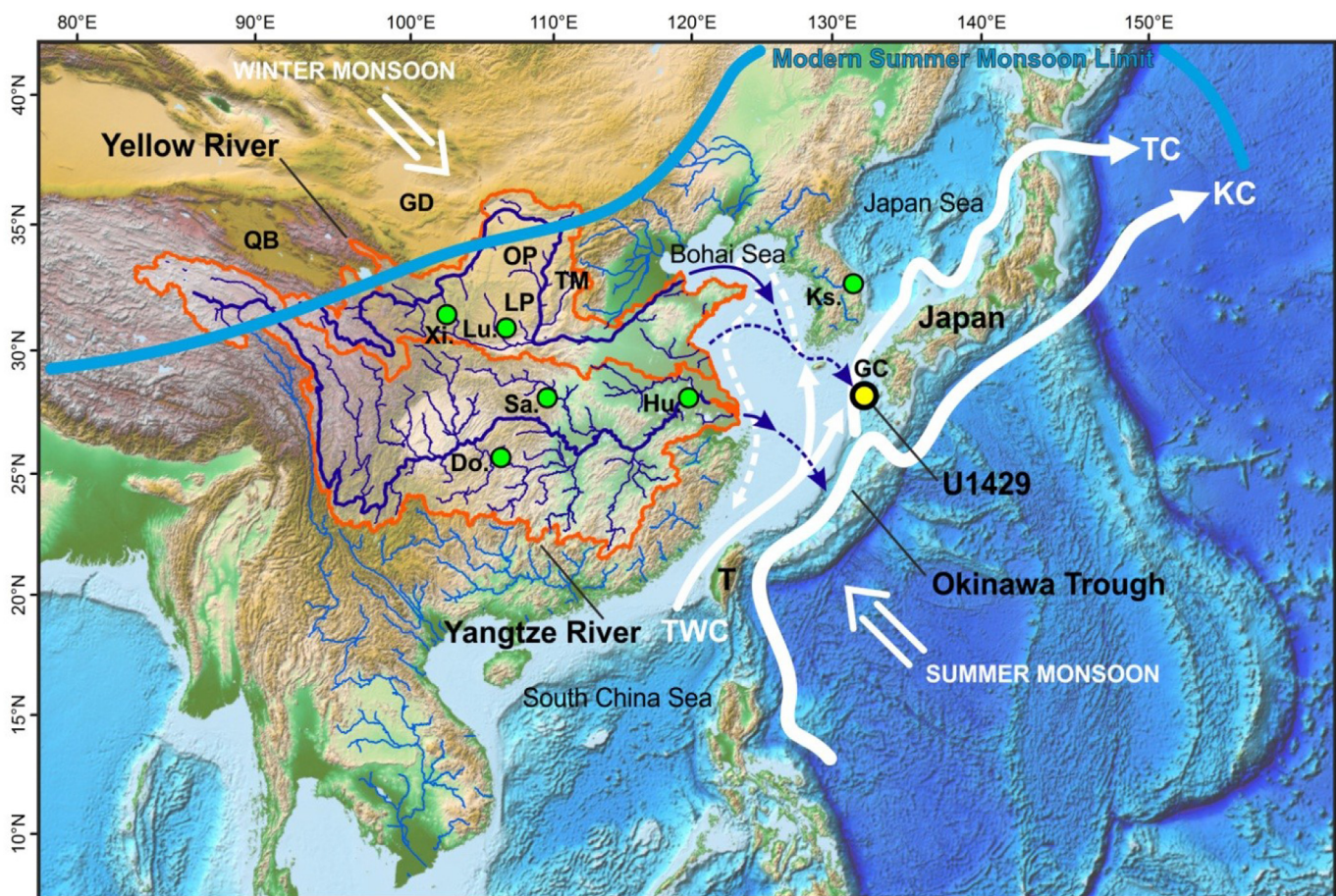


**Fig. 1.** Map of the study area showing the limit of modern summer monsoon front (light blue line; An et al., 2000; Jo et al., 2014), the drainage area of the Yangtze and Yellow rivers (with their glacial lowstand courses, dark blue lines; Ujié and Ujié, 1999; Oiwane et al., 2011; Xu et al., 2014) and the location of Site U1429 (yellow circle; Expedition 346 Scientists, 2014). The thick white arrows depict the regional ocean circulation (TC: Tsushima Current; KC: Kuroshio Current; Lee and Chao, 2003; Liu et al., 2007). The thin white arrows on the East China Sea shelf depict the Taiwan Warm Current (continuous, TWC) and the Yellow Sea Warm Current (dashed), respectively (Lee and Chao, 2003; Liu et al., 2007). The green circles denote the continental sequences (e.g. loess deposits, speleothems) discussed in the text (from West to East: Dongge Cave -Do-, Sanbao Cave -Sa-, Luochuan loess sequence -Lu-, Hulu Cave -Hu-, Korean speleothems -Ks-). Also shown is the location of the Qaidam Basin (QB), Gobi Desert (GD), Ordos Plateau (OP), Loess Plateau (LP), Taihang Mountains (TM), Taiwan (T), and the Goto Submarine Canyon (GC). (For interpretation of the references to color in this figure legend, the reader is referred to the Web version of this article.)

of extensive agricultural activity in the Loess Plateau about 2200 years ago (Milliman et al., 1987). The contribution from Taiwan, estimated from 260 to  $380 \times 10^6$  t/yr for the whole island, is minor in comparison, and only the Lanyang River's sediment ( $\sim 8 \times 10^6$  t/yr) directly entered the southern Okinawa Trough (Huh et al., 2006).

The geological formations of the Yangtze and Yellow river basins provide a diverse array of detrital sediments. The Yangtze river basin hosts volcanic, plutonic, metamorphic, and various Paleozoic to Quaternary sedimentary rocks (Yang et al., 2007). Metamorphic rocks, Cenozoic sedimentary formations, and Quaternary loess characterize the Yellow river Basin (Lin et al., 2001, and references therein).

The alternation of winter (dry, cold) and summer (warm, humid) monsoon-dominated periods characterizes past East Asian monsoons, with their intensities changing in concert with Greenland temperatures and orbitally-driven changes in northern hemisphere summer insolation (Wang et al., 2001, 2008). These hydrological fluctuations influence the dispersal of mineral dust. At present, dust deposits of the Loess Plateau are mainly derived from the Gobi desert (Fig. 1) and other regions of Northwest China. During glacial periods, however, mineral dust from the Loess Plateau likely originated from the Qaidam Basin and the northern Tibetan Plateau (Chen et al., 2007; Sun et al., 2008; Kapp et al., 2011; Pullen et al., 2011). The alternation of these dust sources as principal contributors to the Loess Plateau sediment during the Quaternary is linked to latitudinal shifts in the northern hemisphere Subtropical Jet Stream wind system, which in turn reflects changes in the position of the ITCZ. For example, southward migrations of the subtropical jet stream during glacial periods led to enhanced aridity in Central Asia by decreasing the intensity of the East Asian summer monsoon (Nagashima et al., 2011; Pullen et al., 2011).

## 2.2. Offshore dispersal of the East Asian sediment

The East China Sea is a wide (up to 600 km) and shallow (<120–200 m) epicontinent shelf. It is considered to be a typical example of a river-dominated ocean margin (Liu et al., 2007). Along the shelf, the sediments delivered by the Yangtze and Yellow rivers are dispersed by the northward flowing Kuroshio Current, the Taiwan Warm Current, and the Yellow Sea Warm Current, the latter flowing counter-clockwise in the East China and Yellow Seas (Beardsley et al., 1985; Liu et al., 2007, Fig. 1). Consequently, the sediments discharged from the East Asian rivers are first transported southward along the inner shelf before being routed towards the northeast (Beardsley et al., 1985; Chang et al., 2009). This sediment dispersal pattern was markedly different during glacial intervals when sea level was lower by ~120 m and shallow areas were subaerially exposed (Waelbroeck et al., 2002; Grant et al., 2014). At these times, the East China Sea shelf area was reduced and both the Yangtze and Yellow river mouths were much closer to the Okinawa Trough (Fig. 1). The Yellow river mouth was located east of Cheju Island and fed the Goto Submarine Canyon (Danjo Basin, northern Okinawa Trough), located south of the Goto Islands (southwestern Japan) (Oiwane et al., 2011; Xu et al., 2014). By contrast, the Yangtze River likely fed the middle part of the Okinawa Trough during glacial lowstands (e.g. Ujiié and Ujiié, 1999; Xu et al., 2014). Furthermore, the Kuroshio Current was strongly reduced in strength (e.g. Kao et al., 2006) and shifted eastward out of the Okinawa Trough (Ujiié and Ujiié, 1999; Jian et al., 2000; Ujiié et al., 2003) during glacial periods. Such changes may explain why the Kuroshio Current only impacts sedimentation in the East China Sea during interglacial periods (e.g. Jian et al., 2000; Diekmann et al., 2008).

## 3. Material and methods

### 3.1. The Danjo Basin hemipelagic succession

This study is based on core samples collected during the IODP Expedition 346 (July 29th – September 27th, 2013) at Site U1429 ( $31^{\circ}37.04'N$ ,  $128^{\circ}59.85'E$ , 732 m water depth; Fig. 1). Site U1429 is located in the northernmost part of the East China Sea, more precisely in the southern part of the Okinawa Trough's Danjo Basin. Three holes were drilled at Site U1429 using the advanced piston corer (APC) system to a maximum depth of 188.3 m below the seafloor (mbsf). Hole-to-hole correlations (constrained by the shipboard natural gamma ray, color reflectance, and magnetic susceptibility data) enabled the construction of a spliced section to 188 m composite depth (or CCSF-D, Core Composite depth below Sea Floor). The tephrostratigraphy for U1429, along with the  $\delta^{18}\text{O}$  of benthic foraminifers (Fig. 2), reveals that the sedimentary sequence, mainly composed of olive-gray to greenish gray calcareous nannofossil ooze and calcareous nannofossil-rich clay (Expedition 346 Scientists, 2014), extends from the Middle Pleistocene (~385 ka, MIS 11/10 transition) to the Holocene (Sagawa et al., 2018). Glacial-interglacial variability is constrained together with the  $\delta^{18}\text{O}$ , with the high-resolution (1 cm) Ca/Fe data from XRF scans acquired at the Earth Science Department at ETH Zürich (Fig. 2). Sedimentation rates average ~85 and ~23 cm during glacials and interglacials, respectively. Two centimeters of sediment were sampled every ~4 m for a temporal resolution of ~8 kyr. We avoided sampling visible tephra layers.

### 3.2. Methods

A series of experiments was set up to identify the main phases (i.e. biogenic, detritic, volcanic) of the bulk sediment in order to determine the most relevant grain-size fractions for reconstructing past terrigenous sediment sources at Site U1429. For this purpose, 8 representative samples were selected from glacial and interglacial sediment intervals, including a glass-rich Holocene tephra. Based on scanning electron microscopy (SEM), optical microscopy, and laser grain-size measurements, we elected to focus on the fine sediments (<63  $\mu\text{m}$ ), subdividing the samples into four grain-size fractions: the clay fraction (<2  $\mu\text{m}$ ), the cohesive silty fraction (2–30  $\mu\text{m}$ ), the non-cohesive silty fraction (30–63  $\mu\text{m}$ ), and the bulk fine fraction (0–63  $\mu\text{m}$ ). We measured REE concentrations and Nd isotope ratios for each fraction (Fig. 3).

### 3.3. Sample preparation

The bulk fine fraction of the samples ( $n = 42$ , including the 8 representative samples discussed above) were wet-sieved at 63  $\mu\text{m}$  and 30  $\mu\text{m}$ . The clay and cohesive silt fractions (<2 and 2–30  $\mu\text{m}$ ) were separated by centrifugation (see Bayon et al., 2015 for details). The bulk fine fraction (0–63  $\mu\text{m}$ ) was preserved only for 4 of the representative samples because of the limited amount of sediments. After drying ( $30^{\circ}\text{C}$ ), a sequential extraction procedure was used to remove the non-terrigenous components with the exception of biogenic opal. Biogenic carbonates were removed using a mixture of 10% acetic acid and acetate sodium ( $4 < \text{pH} < 5$ ), Fe–Mn oxyhydroxide phases using hydroxylamine hydrochloride solution, and organic compounds using 5%  $\text{H}_2\text{O}_2$  (Bayon et al., 2002). Note that the REE content in marine opal is quite low compared to corresponding detrital fractions (~3 ppm for Nd; Grouset et al., 1998), so that removal of opal is generally not required prior to Nd isotopic analyses of terrigenous sediments (Bayon et al., 2002). Nevertheless, as a precaution, we focused on samples with limited biogenic silica content (i.e. less than ~10%).

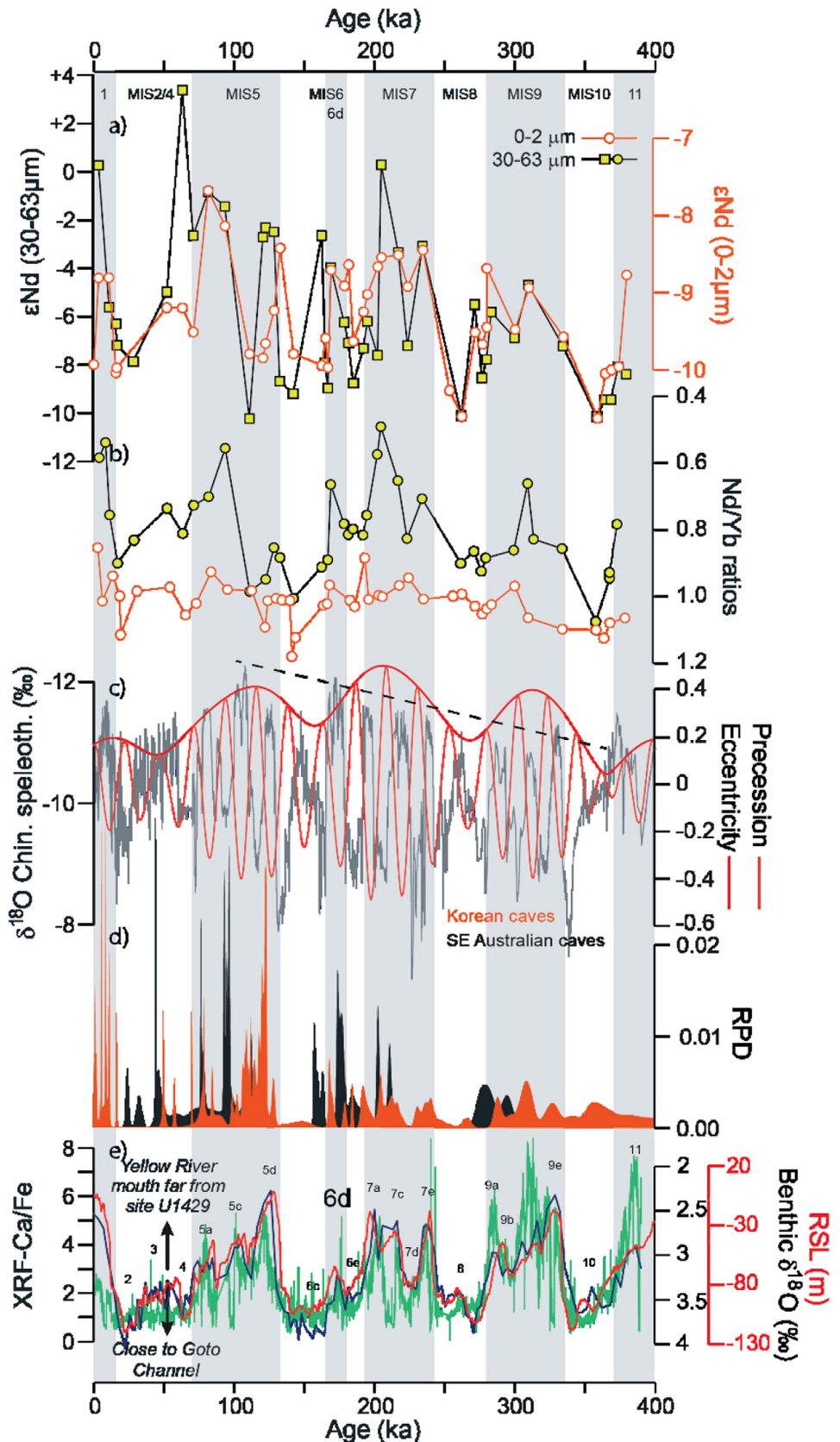


**Fig. 2.** Comparison of U1429 geochemical proxies (i.e., Nd, REE, XRF elemental analysis) with other climate records. Chinese speleothems: [Cheng et al. \(2012, 2016\)](#); Excentricity and precession: [Laskar et al. \(2004\)](#); Relative Probability Density (RPD, speleothem growth): [Jo et al. \(2014\)](#);  $\delta^{18}\text{O}$  of benthic forams from Site U1429: [Sagawa et al. \(2018\)](#); scheme of marine isotope substages (MIS): [Railsback et al. \(2015\)](#).  $\epsilon_{\text{Nd}}$  values of the  $<2 \mu\text{m}$  grain-size fraction exhibit small glacial/interglacial variability ( $\sim 2 \epsilon_{\text{Nd}}$ ) compared to the  $30-63 \mu\text{m}$  grain-size fraction ( $>6 \epsilon_{\text{Nd}}$ ). Both these fractions are characterized by a general trend over the last 400 kyr showing a progressive increase of the interglacial  $\epsilon_{\text{Nd}}$  values. Note that this trend is also visible in the glacial  $\epsilon_{\text{Nd}}$  values from the  $<2 \mu\text{m}$  grain-size fraction. The Nd/Yb ratio of the  $<2 \mu\text{m}$  grain-size fraction stays relatively constant and close to WRAS composition throughout most of the interval. On the other hand, the Nd/Yb ratios of the  $30-63 \mu\text{m}$  grain-size fraction display strong glacial/interglacial variability with lower values during the interglacial periods. Dashed line (c) shows the long term trend visible in the  $\delta^{18}\text{O}$ .

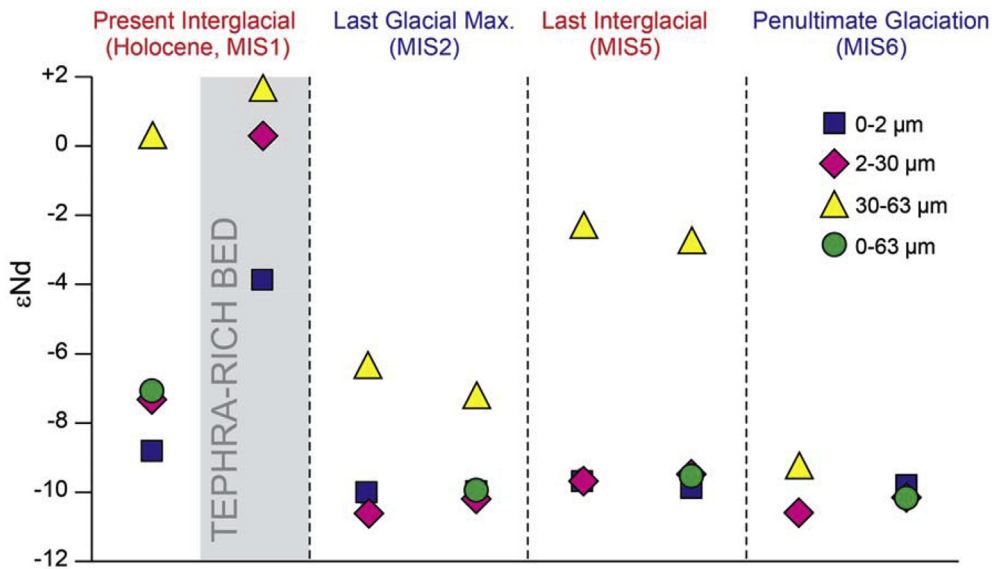


**Fig. 3.** Relationship between  $\epsilon_{\text{Nd}}$  values and grain-size fraction for 8 key samples from Site U1429. Note that we were not able to measure  $\epsilon_{\text{Nd}}$  for the 30–63  $\mu\text{m}$  fraction of the second MIS 6 sample due to a lack of material. All samples from the <2  $\mu\text{m}$ , 2–30  $\mu\text{m}$ , and 0–63  $\mu\text{m}$  fractions are characterized by unradiogenic  $\epsilon_{\text{Nd}}$  values between −11 and −7, whereas the 30–63  $\mu\text{m}$  fraction exhibits high glacial/interglacial variability with unradiogenic values during glacials and radiogenic values during interglacials. Note that the Holocene tephra-rich bed correspond to the Kikai-Akahoya eruption (~7.2 ka) originating from Kyushu island (see [Sagawa et al., 2018](#) and references therein).

### 3.4. Analytical procedure

#### 3.4.1. Rare earth and other trace elements

For trace elements and Nd isotopic analyses, ~100 mg of dry sediment powder was digested by alkaline fusion ([Bayon et al., 2009](#)). This method ensures complete dissolution of sediment samples, including those containing resistant refractory minerals such as zircons, and gives typical blank contributions below the 0.1% level for all elements. Trace element concentrations were measured by ICP-MS (Quad X-Series 2; Thermo Scientific) at the Pôle Spectrométrie Océan, Brest (France). REE abundances were corrected for polyatomic oxide and hydroxide interferences and calculated using the Tm addition method ([Barrat et al., 1996; Bayon et al., 2009](#)). The accuracy of our data was assessed by analysing rock standards and the precision on all measurements was better than 4%, in agreement with the typical precision of alkaline fusion methods (better than 5%; [Bayon et al., 2009](#)).

#### 3.4.2. Neodymium isotopes

Nd was separated using a two-column ion exchange method with AG50W-X8 and Ln resins, as described in the supplementary materials of [Bayon et al. \(2012\)](#). Typical blank levels during the alkaline fusion procedure were generally below 1 ng for Nd and thus negligible (<0.1%) given the large sample sizes of the sediments (between 80 and 100 mg). Isotopic measurements were performed by sample bracketing at the Pôle Spectrométrie Océan (Brest) using a Thermo Scientific Neptune multi-collector ICP-MS. Mass bias corrections on Nd were made with the exponential law, using  $^{146}\text{Nd}/^{144}\text{Nd} = 0.7219$ . Mass-bias corrected values for  $^{143}\text{Nd}/^{144}\text{Nd}$  were normalized to a JNd<sub>i-1</sub> value of  $^{143}\text{Nd}/^{144}\text{Nd} = 0.512115$  ([Tanaka et al., 2000](#)). The average  $^{143}\text{Nd}/^{144}\text{Nd}$  value of JNd<sub>i-1</sub> during our measurements was  $0.512117 \pm 0.000007$ . Analyses of the La Jolla standard solution during the course of this study gave  $^{143}\text{Nd}/^{144}\text{Nd}$  of  $0.511860 \pm 0.000009$  (2 SD, n = 4), agreeing well with the certified value ( $0.511858 \pm 0.000007$ ; [Lugmair et al., 1983](#)) and corresponding to an external reproducibility of  $\sim \pm 0.17\epsilon$  (2 SD). Neodymium isotope data are reported using the epsilon notation,

which corresponds to the deviation of measured  $^{143}\text{Nd}/^{144}\text{Nd}$  ratios relative to the Chondritic Uniform Reservoir (CHUR) value of 0.512638 ([Jacobsen and Wasserburg, 1980](#)).

## 4. Results and discussion

### 4.1. Deciphering the provenance information recorded by the different grain-size fractions

The microscopic observations of the bulk test samples led to the identification of distinct components in the sediments, including biogenic and terrigenous silica, biogenic carbonate clasts (mainly foraminifers), clays, and oxides. In addition, many samples displayed variable amounts of volcanic shards (5–300  $\mu\text{m}$ ; grain-size mode around 40  $\mu\text{m}$ ) and biogenic silica (10–70  $\mu\text{m}$ ; grain-size mode around 15  $\mu\text{m}$ ), mainly concentrated in size-fractions coarser than 10  $\mu\text{m}$ . SEM observations also reveal the presence of heavy minerals such as monazite, titanite, barite, and zircons, each preferentially concentrated in the <10  $\mu\text{m}$  fraction. Evidence of aeolian transport is not observed for the test samples.

Trace elements and  $^{143}\text{Nd}/^{144}\text{Nd}$  isotopic ratios of the analyzed size-fractions are listed in [Table 1](#). Nd concentrations range between 13 and 29 ppm and do not vary as a function of the grain size. Two different types of WRAS-normalized REE patterns (World River Average Silt - WRAS; [Bayon et al., 2015](#)) are distinguishable between the size-fractions. While most of the fractions display relatively flat shale-normalized patterns, the 30–63  $\mu\text{m}$  interglacial sediments are characterized by depletion of the light rare earth elements (LREE) and enrichment of the heavy rare earth elements (HREE) ([Fig. 4](#)). Similarly, while the 0–2, 2–30, and 0–63  $\mu\text{m}$  fractions are characterized by  $\epsilon_{\text{Nd}}$  values ranging from −10.6 to −7.1, the 30–63  $\mu\text{m}$  fraction displays greater Nd isotopic variability and more radiogenic values (reaching −2.7; [Fig. 3](#)). The different size fractions of the glass-rich Holocene sample have more radiogenic Nd isotopic compositions with  $\epsilon_{\text{Nd}}$  values ranging from −3.9 to +1.6.

Our results indicate that the different sediment grain-size fractions have distinct REE and  $\epsilon_{\text{Nd}}$  signatures, hence suggesting

**Table 1**

Nd isotopes and REE compositions (ppm) of the test samples from Site U1429.

sample	size fraction ( $\mu\text{m}$ )	143Nd/144Nd	$2\sigma(10^{-6})$	$\varepsilon_{\text{Nd}}$	La	Ce	Pr	Nd	Sm	Gd	Tb	Dy	Ho	Er	Yb	Lu
A1H1_117	<2	0,512180	8	-8,9	26,3	55,6	6,3	23,1	4,2	3,6	0,5	3,2	0,7	2,0	2,2	0,3
A1H2_119	<2	0,512437	6	-3,9												
A7H6_119	<2	0,512142	6	-9,7	26,7	56,5	6,5	23,1	4,0	3,2	0,5	3,0	0,6	1,9	2,2	0,3
A7H6_70	<2	0,512132	5	-9,9	28,6	60,3	6,8	24,6	4,4	3,6	0,5	3,3	0,7	2,1	2,1	0,3
B2H3_119	<2	0,512122	7	-10,1	22,5	49,6	5,6	19,9	3,5	2,8	0,4	2,6	0,6	1,7	1,9	0,3
B2H4_8	<2	0,512120	8	-10,1	26,4	57,8	6,4	23,0	4,1	3,4	0,5	3,0	0,6	1,9	1,9	0,3
C10H3_118	<2	0,512117	6	-10,2	21,7	48,1	5,3	19,3	3,5	3,0	0,4	2,7	0,5	1,6	1,6	0,2
A1H1_117	2–30	0,512259	8	-7,4	26,4	59,0	6,7	25,1	4,7	4,3	0,7	4,1	0,8	2,5	2,5	0,4
A1H2_119	2–30	0,512655	5	0,3	17,0	42,9	5,1	21,0	4,7	4,8	0,8	5,1	1,1	3,3	3,5	0,5
A7H6_119	2–30	0,512140	8	-9,7	30,6	71,1	7,8	29,0	5,3	4,4	0,7	4,1	0,8	2,4	2,4	0,3
A7H6_70	2–30	0,512154	8	-9,4	27,0	59,2	6,7	24,6	4,5	3,8	0,6	3,5	0,7	2,1	2,1	0,3
B2H3_119	2–30	0,512095	4	-10,6	27,7	61,9	6,9	25,0	4,4	3,7	0,5	3,4	0,7	2,0	2,1	0,3
B2H4_8	2–30	0,512112	6	-10,3	26,9	59,9	6,6	24,1	4,4	3,7	0,6	3,4	0,7	2,0	2,0	0,3
C10H2_119	2–30	0,512094	5	-10,6	14,0	31,9	3,6	13,6	2,5	2,2	0,3	2,0	0,4	1,2	1,2	0,2
C10H3_118	2–30	0,512134	9	-9,8	26,9	59,8	6,6	24,2	4,4	3,9	0,6	3,5	0,7	2,1	2,0	0,3
A1H1_117	30–63	0,512648	5	0,2	17,4	41,7	5,0	20,2	4,6	4,6	0,7	4,8	1,0	3,1	3,2	0,5
A1H2_119	30–63	0,512722	4	1,6	16,5	42,3	5,2	21,4	4,9	5,1	0,8	5,4	1,2	3,5	3,7	0,5
A7H6_119	30–63	0,512520	4	-2,3	27,1	68,5	7,5	26,7	5,1	4,0	0,6	3,7	0,8	2,4	2,6	0,4
A7H6_70	30–63	0,512499	5	-2,7												
B2H3_119	30–63	0,512313	6	-6,3												
B2H4_8	30–63	0,512263	9	-7,3	14,6	31,5	3,5	13,2	2,5	2,4	0,4	2,2	0,5	1,4	1,3	0,2
C10H2_119	30–63	0,512163	7	-9,3												
C10H3_118	30–63	0,512117	8	-10,2	15,1	32,8	3,7	14,0	2,7	2,5	0,4	2,2	0,5	1,3	1,3	0,2
A1H1_117	0–63	0,512268	7	-7,2	24,6	54,6	6,1	23,1	4,4	4,0	0,6	3,7	0,8	2,3	2,4	0,3
A7H6_70	0–63	0,512148	8	-9,6	26,5	57,3	6,5	23,8	4,3	3,7	0,5	3,3	0,7	2,1	2,0	0,3
B2H4_8	0–63	0,512122	9	-10,1	23,9	52,5	5,8	21,2	3,8	3,3	0,5	2,9	0,6	1,7	1,8	0,3
C10H3_118	0–63	0,512499	5	-2,7	23,6	52,6	5,9	21,4	4,0	3,4	0,5	3,1	0,6	1,8	1,8	0,3

that they host distinct sediment sources. During the warm interglacial periods, the non-cohesive silt fraction (30–63  $\mu\text{m}$ ) is characterized by radiogenic  $\varepsilon_{\text{Nd}}$  values (i.e.,  $-2.3 < \varepsilon_{\text{Nd}} < +1.7$ ) and HREE enrichment relative to LREE, suggesting a volcanic origin. The volcanic provenance is also supported by the results obtained for the Holocene tephra level (Kikai-Akahoya, ~7.2 ka) originating from Kyushu island (see Sagawa et al., 2018 and references therein) (Figs. 3 and 4). These geochemical characteristics for the coarse-grained sediments are similar to those of river sediments from Southern Japan ( $\varepsilon_{\text{Nd}} = +2$ ; Fig. 3), representing the dominant radiogenic source in the area. By contrast, the finest (<2  $\mu\text{m}$ ; 2–30  $\mu\text{m}$ ) and coarsest (30–63  $\mu\text{m}$ ) fractions from glacial periods are both characterized by low radiogenic  $\varepsilon_{\text{Nd}}$  values (i.e.,  $-10.6 < \varepsilon_{\text{Nd}} < -6.3$ ) and a WRAS-like REE composition (Figs. 3 and 4). These Nd isotopic compositions suggest mixing between mainland rivers (e.g. Korean, Chinese rivers;  $\varepsilon_{\text{Nd}} < -10$ ) and southern Japanese rivers ( $\varepsilon_{\text{Nd}} > -4$ ). Although the Japanese contribution is not clearly expressed in the REE compositions, our results are independently supported by clay mineral and Sr-Nd-Pb isotopic data for the last glacial-interglacial transition (Zhao et al., 2017, 2018). Indeed, they reveal that the finest size fractions at Site U1429 are predominantly sourced from the Yellow River and southern Japanese rivers, with limited contributions from the Yangtze.

Aeolian contributions at Site U1429 are difficult to quantify. While the Loess Plateau contributes significantly (~90%) to the modern Yellow river sediment load, our geochemical tracers cannot distinguish whether a sediment grain was transported by atmospheric (i.e., dust) or fluvial processes (Yang et al., 2002). Nevertheless, the present-day atmospheric flux of dust in the East China Sea ( $26 \text{ g m}^{-2} \text{ yr}^{-1}$ ), comparable to late Quaternary records of aeolian dust accumulation (Gao et al., 1997), composes only ~4–6% of the terrigenous sediment flux at U1429 during the last glacial (up to  $60 \text{ g cm}^{-2} \text{ kyr}^{-1}$ ; Zhao et al., 2017). Moreover, the impact of aeolian transport on our geochemical investigations is restricted to the clay-sized fraction because the mean grain-size of dust particles reaching the modern China Sea is ~1.9  $\mu\text{m}$  (Gao et al., 1997). This is

supported by the absence of aeolian morphologies for the U1429 silt grains observed through SEM. We thus conclude that the impact of dust inputs at Site U1429, although not negligible, is low over the studied period. Likewise, we conclude that Taiwanese sediments are not present at Site U1429 in appreciable quantities due to a lack of LREE enrichment (Diekmann et al., 2008; Dou et al., 2010, 2012; Zhao et al., 2017, 2018). The lack of Taiwanese sediment transport to the Danjo Basin is probably due to the outflow of the Kuroshio Current from the Okinawa Trough south of the Ōsumi archipelago (i.e. Tokara Strait), ~300 km south of Site U1429 (e.g. Feng et al., 2000, Fig. 1).

Based on results from the eight test samples, we focus on the clay (<2  $\mu\text{m}$ ) and non-cohesive silt (30–63  $\mu\text{m}$ ) fractions to investigate past provenance changes at Site U1429. The clay fraction has minimal contamination from volcanic shards and biogenic silica. This fraction was previously analyzed to discern past variations in the discharge of river-borne detrital sediments from the Yellow river and Japanese rivers (Zhao et al., 2017, 2018). The non-cohesive silt fraction will provide insights into the evolution of paleoclimatic conditions in Japan. We excluded samples with large numbers of volcanic shards from the paleoclimatic reconstruction in order to separate volcanic eruptions from broader changes in regional climate.

#### 4.2. The past 400 kyr: focusing on the 0–2 $\mu\text{m}$ and 30–63 $\mu\text{m}$ grain-size fractions

Throughout the last 400 kyr, Nd concentrations range between 13 and 29 ppm for the clay fraction, and between 11 and 27 ppm for the non-cohesive silty fraction (Table 2). The Nd/Yb ratio, a measure of HREE enrichment, is commonly used to discriminate the provenance of sediments. Shale-normalized Nd/Yb ratios ( $\text{Nd}/\text{Yb})_{\text{N}}$  close to 1 are typical of the upper continental crust, whereas  $(\text{Nd}/\text{Yb})_{\text{N}}$  ratios of less than 1 may indicate the presence of volcanic materials (Bayon et al., 2015). In Site U1429 sediments, the clay fraction is characterized by  $(\text{Nd}/\text{Yb})_{\text{N}}$  ratios ranging from 0.83 to 1.15 (Table 2), exhibiting REE patterns without particular enrichment or depletion

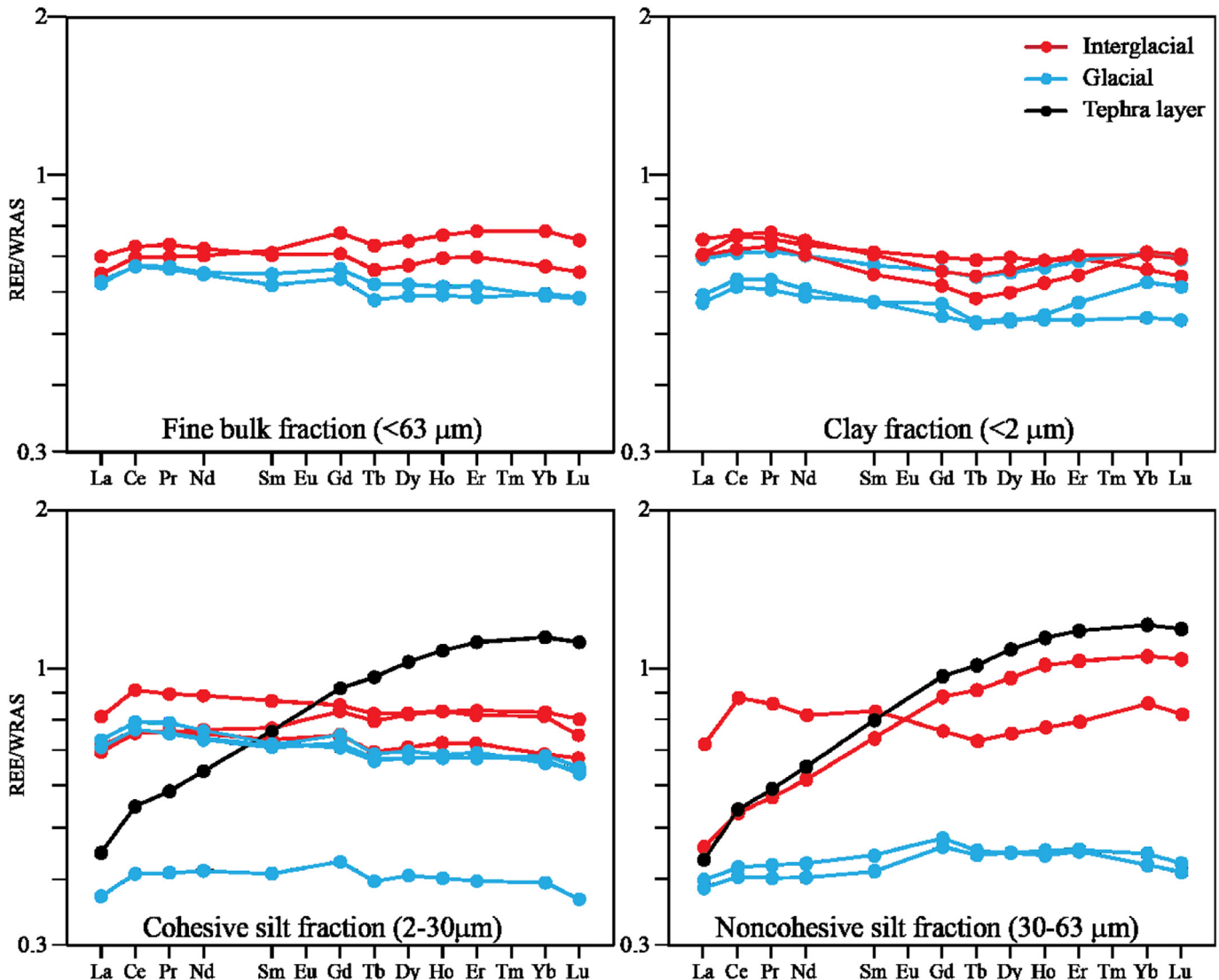


**Fig. 4.** WRAS-normalized REE compositions of test samples at Site U1429. WRAS: World River Average Silts. Note that less samples have been analyzed in the coarse fractions ( $0\text{--}63\,\mu\text{m}$  and  $30\text{--}63\,\mu\text{m}$ ) due to the paucity of certain sediments. For similar reasons, REE analyses were not performed on the  $0\text{--}63\,\mu\text{m}$  size fraction of the tephra sample. Priority was given to Nd isotopes in all cases. All glacial samples exhibit REE patterns similar to the WRAS composition. Interglacial sample REE compositions are similar to the glacial samples for the  $<2\,\mu\text{m}$ ,  $2\text{--}30\,\mu\text{m}$ , and  $0\text{--}63\,\mu\text{m}$  grain-size fractions, but are more similar to the tephra sample in the  $30\text{--}63\,\mu\text{m}$  grain-size fraction, thus indicating Japanese provenance. In all grain-size fractions, the REE-depleted character of the glacial samples is more pronounced than for interglacial samples due to higher biogenic silica (characterized by very low REE concentration) content in the former.

relative to the average continental sediments. The non-cohesive silt fraction ( $30\text{--}63\,\mu\text{m}$ ), however, is characterized by a significantly lower ( $\text{Nd/Yb})_N$  ratios from 0.49 to 1.08 (Fig. 2b). These lower values suggest the incorporation of substantial amounts of volcanic sediments from Japan. While the ( $\text{Nd/Yb})_N$  of the clay fraction remains relatively constant throughout the studied interval, the ( $\text{Nd/Yb})_N$  ratios of the non-cohesive silts tracks the glacial/interglacial cyclicity, with higher values recorded during glacial intervals (Fig. 2b).

The  $\varepsilon_{\text{Nd}}$  values of the clay fraction vary between  $-10.7$  and  $-6.2$  through the studied period, with most radiogenic values corresponding to the interglacials. While the non-cohesive silt  $\varepsilon_{\text{Nd}}$  values are more variable, with  $\varepsilon_{\text{Nd}}$  ranging from  $-10.3$  to  $+3.4$ , the most radiogenic values are also found during the interglacials (Fig. 2a). We also notice a progressive increase in the mean  $\varepsilon_{\text{Nd}}$  throughout the last 400 kyr. Over the entire interval, this rise corresponds to a positive  $\varepsilon_{\text{Nd}}$  shift of  $1.2 \pm 0.2$  for the clay fraction and  $5 \pm 3$  for the non-cohesive silt fraction (Fig. 2a).

#### 4.3. Sediment provenance at site U1429

Results from the past 400 kyr are consistent with the recent results of Zhao et al. (2017, 2018) that suggest two dominant sediment sources at U1429. Both the fine fractions ( $0\text{--}2\,\mu\text{m}$  and  $2\text{--}30\,\mu\text{m}$ ) show unradiogenic  $\varepsilon_{\text{Nd}}$  and WRAS-like REE patterns suggesting a Yellow river source ( $-13.9 < \varepsilon_{\text{Nd}} < -9.6$ ;  $\text{Nd/Yb} \approx 1$ ; Figs. 2, 5 and 6, Table 3) with minor contributions from southern Japanese rivers ( $\varepsilon_{\text{Nd}} > -2$ ;  $\text{Nd/Yb} \ll 1$ ; Figs. 5 and 6, Table 3). The provenance of the non-cohesive silt fraction  $\varepsilon_{\text{Nd}}$  and  $(\text{Nd/Yb})_N$  is less clear. During glacial periods, the combination of their unradiogenic  $\varepsilon_{\text{Nd}}$  values, high ( $\text{Nd/Yb})_N$  ratios and WRAS-like REE patterns may indicate a dominant Yellow river provenance, but during interglacials the more radiogenic  $\varepsilon_{\text{Nd}}$  compositions, lower ( $\text{Nd/Yb})_N$  ratios, and HREE enrichment suggests an increased contribution of volcanic material. These observations imply varying relative contributions from Yellow river (-dominant) and southern Japan (-dominant) sediment sources to the non-cohesive

**Table 2** $\epsilon_{\text{Nd}}$  and REEs of the Site U1429 sediments.

sample	age (ka)	143Nd/144Nd	$2\sigma(10^{-6})$	$\epsilon_{\text{Nd}}$	(Nd/Yb)N	La	Ce	Pr	Nd	Sm	Gd	Tb	Dy	Ho	Er	Yb	Lu
<b>0–2 <math>\mu\text{m}</math> size fraction</b>																	
A1H1_5	0,2	0,512128	7	-10,0	0,83	44,5	39,8	4,6	16,4	2,9	2,3	0,4	2,3	0,5	1,6	1,8	0,3
A1H1_117	3,7	0,512180	8	-8,8	0,99	26,3	55,6	6,3	23,1	4,1	3,6	0,5	3,2	0,7	2,0	2,2	0,3
A1H3_119	11,1	0,512186	7	-8,8	0,91	28,0	50,4	5,7	20,4	3,6	3,1	0,5	2,9	0,6	1,9	2,1	0,3
B2H3_119	16,0	0,512122	7	-10,1	0,97	22,5	49,6	5,6	19,9	3,5	2,8	0,4	2,6	0,6	1,7	1,9	0,3
B2H4_8	16,7	0,512120	8	-10,0	1,09	26,4	57,8	6,4	23,0	4,1	3,4	0,5	3,0	0,6	1,9	1,9	0,3
A2H6_119	28,5			0,96		26,7	56,8	6,2	22,2	3,9	2,8	0,5	3,2	0,7	2,0	2,1	0,3
B4H6_119	52,3	0,512164	9	-9,2	0,95	24,9	53,9	5,9	21,3	3,8	2,8	0,5	3,0	0,6	1,9	2,1	0,3
B5H3_118	63,4	0,512166	6	-9,2	1,03	27,4	51,4	5,7	20,5	3,7	3,1	0,5	2,8	0,6	1,7	1,8	0,3
B5H6_7	71,2	0,512149	7	-9,5	0,99	22,4	44,3	4,9	17,4	3,0	2,5	0,4	2,4	0,5	1,5	1,6	0,2
B6H2_119	81,9	0,512244	6	-7,7	0,90	21,7	42,6	4,8	17,4	3,1	2,6	0,4	2,5	0,5	1,7	1,8	0,3
C8H1_9	93,8	0,512221	6	-8,1	0,95	24,2	47,4	5,4	19,8	3,5	3,0	0,5	2,8	0,6	1,8	1,9	0,3
A7H4_110	111,2	0,512135	5	-9,8	0,96	25,1	48,8	5,5	19,6	3,3	2,7	0,4	2,6	0,6	1,8	1,9	0,3
A7H6_70	120,8	0,512132	5	-9,9	1,07	28,6	60,3	6,8	24,6	4,3	3,6	0,5	3,3	0,7	2,1	2,1	0,3
A7H6_119	122,8	0,512142	6	-9,7	0,99	26,7	56,5	6,5	23,1	4,0	3,2	0,5	3,0	0,6	1,9	2,2	0,3
B8H3_119	128,7	0,512164	6	-9,2	0,98	18,1	34,0	3,9	13,8	2,4	2,0	0,3	1,9	0,4	1,3	1,3	0,2
B8H4_119	132,9	0,512206	5	-8,4	0,98	23,6	44,6	5,0	18,1	3,2	2,7	0,4	2,5	0,5	1,6	1,7	0,3
B8H6_7	138,7	0,512322	4	-6,1	0,98	21,0	41,8	4,8	17,4	3,2	2,7	0,4	2,5	0,5	1,6	1,6	0,2
C10H2_119	140,1			1,15		27,3	62,5	6,9	25,4	4,5	3,8	0,6	3,5	0,7	2,0	2,0	0,3
C10H3_118	142,6	0,512117	6	-9,8	1,10	21,7	48,1	5,3	19,3	3,4	3,0	0,4	2,7	0,5	1,6	1,6	0,2
B10H3_119	162,8	0,512127	6	-10,0	1,00	25,0	51,3	5,7	20,2	3,6	2,9	0,4	2,7	0,6	1,8	1,9	0,3
B10H4_118	165,5	0,512145	6	-9,6	0,99	24,4	48,7	5,4	19,4	3,4	2,8	0,4	2,7	0,6	1,7	1,8	0,3
A10H3_8	167,3	0,512126	7	-10,0	0,94	23,1	45,0	5,1	18,0	3,1	2,5	0,4	2,5	0,5	1,7	1,8	0,3
A10H3_119	169,3	0,512191	4	-8,7													
B11H2_97	178,9	0,512180	3	-8,9	0,98	24,2	47,4	5,4	19,1	3,3	2,7	0,4	2,6	0,6	1,7	1,8	0,3
B11H3_119	181,9	0,512194	5	-8,7	1,00	26,7	56,0	6,2	22,1	3,8	3,2	0,5	2,9	0,6	1,9	2,0	0,3
B11H5_9	185,3	0,512143	7	-9,7	0,86	21,8	37,0	4,3	15,0	2,6	2,1	0,3	2,1	0,5	1,4	1,6	0,2
B11H6_9	192,6	0,512163	6	-9,3	0,98	23,3	45,3	5,1	18,4	3,2	2,6	0,4	2,5	0,5	1,7	1,7	0,3
B11H6_119	195,3	0,512175	7	-9,0	0,97	25,2	49,4	5,6	20,1	3,5	2,9	0,4	2,8	0,6	1,8	1,9	0,3
C13H5_9	202,6	0,512193	5	-8,7	0,97	27,0	53,6	6,3	22,9	4,2	3,7	0,5	3,4	0,7	2,1	2,2	0,3
C13H5_119	205,2	0,512200	4	-8,6	0,94	23,6	46,2	5,3	19,2	3,5	2,9	0,4	2,8	0,6	1,8	1,9	0,3
A12H3_119	217,4	0,512201	7	-8,5	0,92	21,0	39,8	4,5	16,3	2,9	2,4	0,4	2,3	0,5	1,5	1,6	0,2
A12H5_118	224,0	0,512180	5	-8,9	0,98	25,1	49,3	5,6	19,8	3,4	2,9	0,4	2,8	0,6	1,8	1,9	0,3
B13H7_9	234,8	0,512205	6	-8,5	0,97	23,7	45,5	5,2	18,6	3,2	2,7	0,4	2,5	0,5	1,6	1,8	0,3
B16H3_119	253,9	0,512110	6	-10,3	0,97	24,0	47,3	5,4	19,1	3,4	2,7	0,4	2,6	0,6	1,7	1,8	0,3
B16H5_119	262,5	0,512093	5	-10,6	1,00	25,3	47,1	5,4	18,8	3,1	2,5	0,4	2,4	0,5	1,6	1,7	0,3
C18H5_118	272,0	0,512149	5	-9,5	1,03	25,4	50,6	5,8	20,6	3,6	3,0	0,4	2,8	0,6	1,8	1,8	0,3
B17H2_119	277,3	0,512141	5	-9,7	1,01	25,4	49,6	5,6	20,4	3,6	3,0	0,5	2,8	0,6	1,8	1,9	0,3
B17H3_118	280,4	0,512153	6	-9,5	1,00	27,0	53,7	6,1	22,0	3,9	3,3	0,5	3,1	0,7	2,0	2,0	0,3
B17H4_119	280,4	0,512192	5	-8,7	0,94	26,1	52,1	6,0	22,2	4,1	3,7	0,6	3,4	0,7	2,1	2,2	0,3
C19H6_8	300,4	0,512151	5	-9,5	1,04	26,3	53,0	6,0	22,2	4,0	3,4	0,5	3,1	0,7	1,9	2,0	0,3
B18H3_119	310,3	0,512179	7	-8,9	1,07	25,0	51,1	5,8	20,7	3,8	3,1	0,5	2,8	0,6	1,8	1,8	0,3
B19H1_119	334,9	0,512146	3	-9,6	1,07	24,2	49,7	5,6	20,1	3,6	3,0	0,5	2,7	0,6	1,7	1,7	0,2
A20H2_119	359,2	0,512092	7	-10,7	1,10	26,5	54,5	6,1	21,8	3,9	3,1	0,5	2,9	0,6	1,8	1,8	0,3
A20H4_9	364,8	0,512122	7	-10,1	1,05	25,2	51,6	5,8	21,1	3,9	3,2	0,5	2,9	0,6	1,8	1,8	0,3
A20H5_7	369,1	0,512124	5	-10,0	1,04	25,1	51,6	5,8	21,2	3,8	3,2	0,5	3,0	0,6	1,8	1,9	0,3
B20H3_119	374,4	0,512126	5	-10,0													
B20H5_8	379,9	0,512188	6	-8,8	1,04	24,6	49,7	5,7	20,7	3,8	3,2	0,5	3,0	0,6	1,9	2,0	0,3
<b>30–63 <math>\mu\text{m}</math> size fraction</b>																	
A1H1_117	3,7	0,512648	5	0,3	0,58	17,4	41,7	5,0	20,2	4,5	4,6	0,7	4,8	1,0	3,1	3,2	0,5
A1H2_119	8,1	0,512722	4	-3,9	0,54	16,5	42,3	5,2	21,4	4,9	5,1	0,8	5,4	1,2	3,5	3,7	0,5
A1H3_119	11,1	0,512230	9	-5,6	0,76	18,4	38,1	4,3	16,2	3,2	2,6	0,5	2,9	0,6	1,9	2,0	0,3
B2H3_119	16,0	0,512313	6	-6,3													
B2H4_8	16,7	0,512263	9	-7,2	0,90	14,6	31,5	3,5	13,2	2,5	2,4	0,4	2,2	0,5	1,4	1,3	0,2
A2H6_119	28,5	0,512230	9	-7,9	0,83	14,2	28,6	3,2	12,0	2,3	1,9	0,3	2,0	0,4	1,3	1,3	0,2
B4H6_119	52,3	0,512380	10	-5,0	0,74	15,6	27,7	3,2	12,4	2,4	2,0	0,3	2,1	0,4	1,4	1,5	0,2
B5H3_118	63,4	0,512460	8	3,4	0,81	17,5	36,3	4,2	16,1	3,1	2,6	0,4	2,7	0,6	1,7	1,8	0,3
B5H6_7	71,2	0,512500	7	-2,7	0,73	17,6	37,8	4,4	17,0	3,5	3,0	0,5	3,2	0,7	2,0	2,2	0,3
B6H2_119	81,9	0,512594	9	-0,8	0,70	20,7	45,3	5,3	20,2	4,1	3,5	0,6	3,8	0,8	2,5	2,6	0,4
C8H1_9	93,8	0,512563	9	-1,4	0,56	19,5	44,9	5,4	21,5	4,9	4,8	0,8	5,3	1,1	3,4	3,6	0,5
A7H4_110	111,2	0,512107	13	-10,3	0,99	26,0	35,5	4,1	15,7	2,8	2,3	0,4	2,3	0,5	1,4	1,5	0,2
A7H6_70	120,8	0,512499	5	-2,7													
A7H6_119	122,8	0,512520	4	-2,3	0,95	27,1	68,5	7,5	26,7	4,7	4,0	0,6	3,7	0,8	2,4	2,6	0,4
B8H3_119	128,7	0,512508	7	-2,5	0,85	16,9	36,6	4,3	16,7	3,3	2,9	0,5	2,9	0,6	1,8	1,8	0,3
B8H4_119	132,9	0,512500	6	-8,8	0,88	14,2	30,8	3,7	14,1	2,8	2,3	0,4	2,3	0,5	1,4	1,5	0,2
C10H3_118	142,6	0,512117	8	-9,3	1,01	15,1	32,8	3,7	14,0	2,7	2,5	0,4	2,2	0,5	1,3	1,3	0,2
B10H3_119	162,8	0,512187	9	-2,7	0,91	12,0	27,2	3,2	12,1	2,3	1,8	0,3	1,9	0,4	1,2	1,2	0,2
B10H4_118	165,5	0,512228	9	-8,0	0,82	12,3	27,3	3,2	11,9	2,2	1,8	0,3	2,0	0,4	1,3	1,3	0,2

**Table 2** (continued)

sample	age (ka)	$^{143}\text{Nd}/^{144}\text{Nd}$	$2\sigma(10^{-6})$	$\varepsilon_{\text{Nd}}$	(Nd/Yb)N	La	Ce	Pr	Nd	Sm	Gd	Tb	Dy	Ho	Er	Yb	Lu
B11H6_119	195,3	0,512317	8	-6,2	0,76	15,0	34,4	4,0	15,1	3,0	2,5	0,4	2,8	0,6	1,8	1,8	0,3
C13H5_9	202,6	0,512500	9	-7,7	0,57	15,0	37,1	4,4	17,3	3,8	3,6	0,6	4,1	0,9	2,7	2,8	0,4
C13H5_119	205,2	0,512652	5	0,3	0,49	13,6	34,7	4,2	17,3	4,0	4,0	0,7	4,6	1,0	3,1	3,2	0,5
A12H3_119	217,4	0,512464	9	-3,4	0,65	12,9	29,6	3,4	12,9	2,6	2,2	0,4	2,6	0,6	1,7	1,8	0,3
A12H5_118	224,0	0,512264	8	-7,3	0,83	13,9	31,1	3,5	12,8	2,4	1,9	0,3	2,1	0,4	1,3	1,4	0,2
B13H7_9	234,8	0,512478	8	-3,1	0,71	16,3	37,4	4,0	14,3	2,6	2,1	0,4	2,4	0,5	1,6	1,9	0,3
B16H5_119	262,5	0,512114	6	-10,2	0,90	14,9	32,3	3,7	13,6	2,5	1,9	0,3	2,1	0,4	1,4	1,4	0,2
C18H5_118	272,0	0,512353	7	-5,5	0,86	17,5	40,5	4,7	17,6	3,4	2,7	0,5	2,9	0,6	1,8	1,9	0,3
B17H2_119	277,3	0,512194	8	-8,6	0,92	20,6	42,4	4,8	17,6	3,2	2,6	0,4	2,7	0,6	1,8	1,8	0,3
B17H3_118	280,4	0,512235	5	-7,8	0,89	19,4	43,7	5,0	18,2	3,4	2,6	0,5	2,8	0,6	1,8	1,9	0,3
C19H6_8	300,4	0,512281	6	-6,9	0,86	17,3	38,1	4,3	15,9	3,0	2,4	0,4	2,6	0,6	1,7	1,7	0,3
B18H3_119	310,3	0,512395	7	-4,7	0,66	15,5	36,0	4,2	15,7	3,2	2,7	0,5	3,0	0,7	2,0	2,2	0,3
B18H4_119	314,7	0	0		0,83	16,5	37,1	4,3	16,1	3,1	2,6	0,4	2,7	0,6	1,7	1,8	0,3
B19H1_119	334,9	0,512263	7	-7,3	0,86	15,3	34,9	4,0	14,9	2,9	2,3	0,4	2,4	0,5	1,6	1,6	0,2
A20H2_119	359,2	0,512111	7	-10,2	1,08	17,3	37,6	4,3	15,4	2,9	2,2	0,4	2,2	0,5	1,3	1,3	0,2
A20H4_9	364,8	0,512148	8	-9,5	0,96	18,5	40,0	4,5	16,7	3,1	2,5	0,4	2,7	0,6	1,7	1,6	0,2
A20H5_7	369,1	0,512149	6	-9,5	0,95	20,4	45,6	5,1	19,1	3,6	2,6	0,5	2,8	0,6	1,8	1,9	0,3
A20H5_8	369,2	0,512203	8	-9,5	0,93	18,6	41,7	4,7	17,4	3,3	2,6	0,4	2,7	0,6	1,7	1,7	0,3
B20H3_119	374,4	0,512218	6	-8,2	0,78	15,1	33,2	3,8	14,2	2,7	2,1	0,4	2,4	0,5	1,6	1,7	0,2

silt fractions during glacial and interglacial periods, respectively. The  $\varepsilon_{\text{Nd}}$  value of -5 represents a threshold for the REE patterns, with samples having  $\varepsilon_{\text{Nd}}$  less than -5 being characterized by WRAS-like composition (i.e. upper continental crust) and samples with  $\varepsilon_{\text{Nd}}$  greater than -5 more closely reflecting volcanic compositions (Fig. 6).

#### 4.4. Glacial/interglacial variations

During the last 400 kyr, the  $\varepsilon_{\text{Nd}}$  values of the clay and non-cohesive silts vary in phase with the glacial-interglacial cyclicity (Fig. 2). This variability reflects the fluctuating contributions from southern Japanese and Yellow rivers sediments to the northern tip of the Okinawa Trough. As discussed in Section 4.3, the coarser fraction is dominated by the Yellow river during glacial periods and by southern Japanese rivers during interglacial periods. Lowstand conditions and the associated eastward migration of the Yellow River delta towards Site U1429 during glacial intervals (Oiwane et al., 2011) likely explain the increasing contributions of Yellow River sediments to this coarser fraction. Since the Yangtze river mouth has migrated towards the Middle Okinawa Trough during glacials (Ujiiie et al., 1991), it did not contribute significantly to glacial sedimentation at Site U1429 (Zhao et al., 2017, 2018). Similarly, sea level rise of about 100–130 m (Waelbroeck et al., 2002; Grant et al., 2014) involves a westward migration of the Yellow river delta of about 1000 km and the appearance of the Yellow Sea warm current onto the East China Sea shelf. The combination of the Yellow river delta migration with the significant change in the regional oceanic circulation likely explains the decreasing contribution of the Yellow River to the non-cohesive silt fraction at glacial-interglacial transitions. In addition, significant inputs of Japanese sources during interglacials could have occurred in response to increasing rainfall over Japan in response to the northward movement of the ITCZ (e.g. Xiao et al., 1999; Jo et al., 2014). For an analogy in terms of modern atmospheric processes, precipitation over Japan is more likely during summer. Enhanced precipitation may have led to an increase in Japanese river basin erosion (Xiao et al., 1999), favouring the transport of sediments to the Danjo basin. Therefore,  $\varepsilon_{\text{Nd}}$  changes observed in the non-cohesive silt fraction provide important insights on the factors driving the supplies of terrigenous sediments to Site U1429 through the studied period. More specifically, our results demonstrate that the regional rainfall patterns over the East Asian continent and the Japanese islands, as well as sea level changes, drive the transfer of continental sediments to the northern tip of the Okinawa Trough over the last 400 kyr.

In contrast, the  $\varepsilon_{\text{Nd}}$  composition of the clay fraction through the last 400 kyr is mostly controlled by contribution from Yellow River inputs (Section 4.3). One can assume that both sea-level variations and changes of the monsoonal rainfall pattern could explain the glacial/interglacial  $\varepsilon_{\text{Nd}}$  variability observed in this finest fraction (see the above discussion). However, considering the complexity of East Asian mainland geology, an alternative hypothesis may be that these  $\varepsilon_{\text{Nd}}$  changes reflect rainfall variability occurring within the drainage basin of the Yellow river in response to latitudinal shifts of the ITCZ. In fact, it is well known that present-day loess deposits from the northern-central part of the Yellow river are the main contributors of the Yellow river sediments discharges (Saito et al., 2001 and references therein; Yang et al., 2002; Hu et al., 2012). The Loess Plateau is characterized by  $\varepsilon_{\text{Nd}}$  signatures ranging from -12 to -7 (Table 3). This range of values is consistent with the  $\varepsilon_{\text{Nd}}$  recorded in the clay fraction deposited at Site U1429 (Figs. 2 and 5), validating the hypothesis that the Loess Plateau controls the terrigenous sediment flux of the Yellow river sediment discharge over the last 400 kyr. The Nd isotopic signatures of the Chinese loess deposits are not geographically homogenous, however. For example, loess sequences encountered at the Ordos Plateau, north of the Loess Plateau (Fig. 1), exhibit less radiogenic Nd isotopic signatures (from -21 to -10; Table 3), and increasing inputs from this source to the Yellow River discharge during glacial periods could explain the observed  $\varepsilon_{\text{Nd}}$  changes. At present, the Ordos Plateau is located at the northern end of the modern summer monsoon front (Fig. 1) and receives little precipitations (100–450 mm/yr) relative to the Loess Plateau (600–1000 mm/yr; Porter et al., 2001; Xu et al., 2010). In addition, dry-and-cold winter monsoon conditions prevailed during glacial intervals (e.g. An et al., 1990, 2000; Rousseau et al., 2009; Jo et al., 2014). Consequently, if enhanced rainfall (and associated soil erosion) can increase the contribution of the Loess Plateau to the Yellow river sediment discharge under summer monsoon dominated interglacial conditions, aeolian processes are considered as the main driver to transport loess particles from the Ordos Plateau to the Yellow River (west of the Taihang Mountains in particular) during glacial periods (Hu et al., 2012). Thus, the monsoon regime and, by extension, the latitudinal ITCZ shifts could explain the ~2  $\varepsilon_{\text{Nd}}$  glacial-interglacial difference observed in the geochemical signatures of the clay sediments deposited at Site U1429. Enhanced dust inputs from the Ordos Plateau to the East China Sea, although difficult to quantify, certainly reinforce the glacial  $\varepsilon_{\text{Nd}}$  signature of clays observed at U1429. Nevertheless, the riverine contribution is strongly supported by the ~2  $\varepsilon_{\text{Nd}}$  shifts observed between glacial and

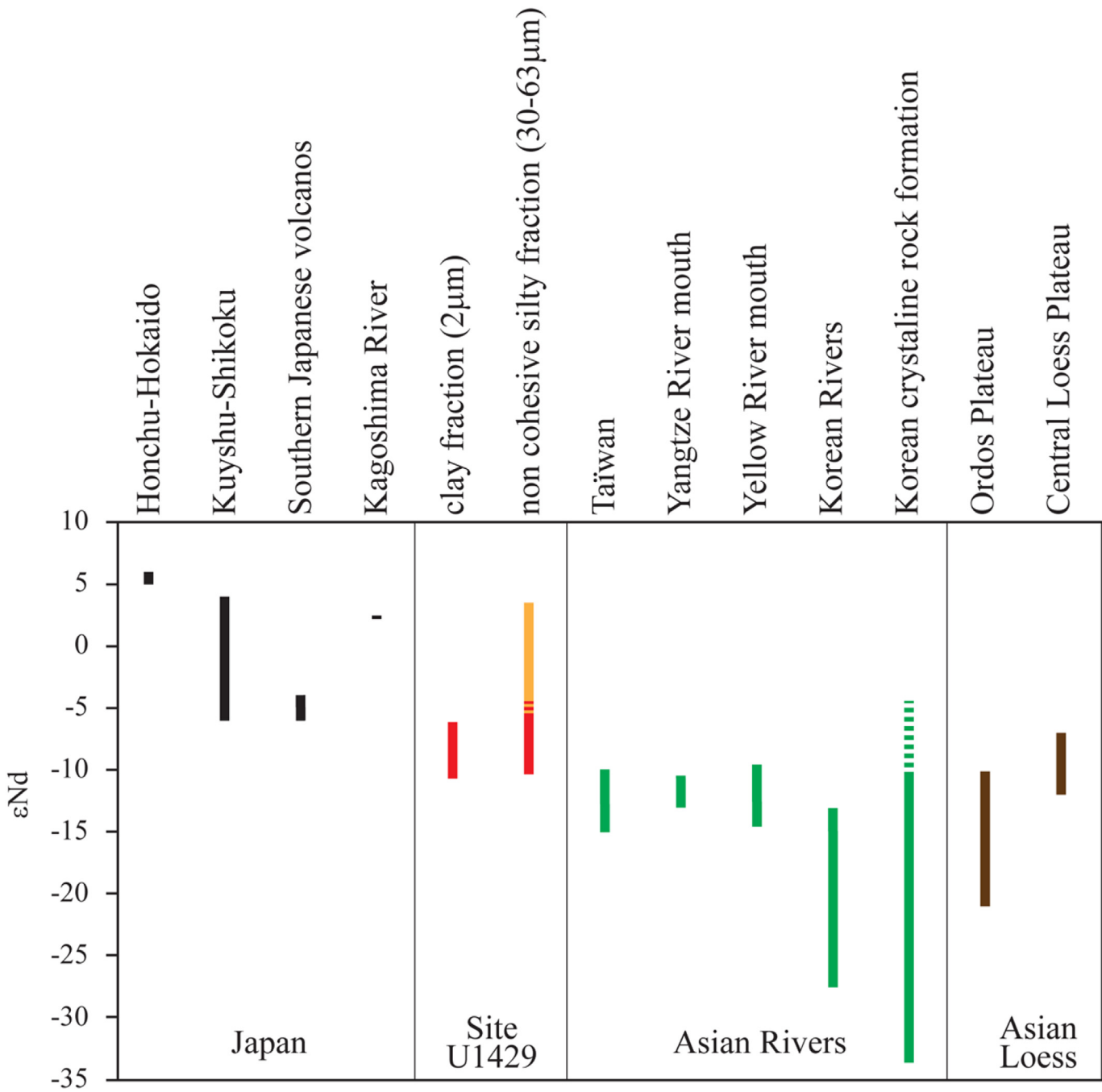


**Fig. 5.**  $\varepsilon_{\text{Nd}}$  values of sediments from Site U1429 and potential sources (see Table 3 for detailed references). Red corresponds to the samples from Site U1429 characterized by WRAS-like REE patterns, whereas orange represents the samples with a typical volcanic signature (i.e. southern Japanese rivers) in both Nd isotopes and REE composition. (For interpretation of the references to color in this figure legend, the reader is referred to the Web version of this article.)

interglacial intervals (more precisely MIS 1 to 4) in the sediment from the modern Yellow river delta, with contributions from the Ordos Plateau increasing during MIS 2 and MIS 4 (Hu et al., 2012). The use of additional provenance proxies (e.g.  $^{87}\text{Sr}/^{86}\text{Sr}$  ratios; clay mineralogy) could help further constrain sediment sources and test the aforementioned hypotheses. Regardless of the exact sources responsible for the observed changes, the glacial/interglacial  $\varepsilon_{\text{Nd}}$  variability (and the recorded radiogenic nature of the interglacial periods in particular) appears to reflect not only sea-level variations and associated changes in oceanic circulation, but also changes in regional rainfall patterns over the study area. This is particularly

well supported by the  $\varepsilon_{\text{Nd}}$  variability observed within the MIS 6 glacial period, specifically during MIS 6d (Fig. 2; Section 4.5).

#### 4.5. Zooming in on MIS 6

The systematic glacial-interglacial  $\varepsilon_{\text{Nd}}$  variability (i.e., more radiogenic values during interglacial intervals) identified through the last 400 kyr at Site U1429 (Fig. 2) is particularly clear for MIS 6 (and more specifically during the interval between ca. 150–180 ka, i.e., MIS 6d). As discussed previously, the non-cohesive silt fraction displays interglacial  $\varepsilon_{\text{Nd}}$  and REE characteristics that suggest

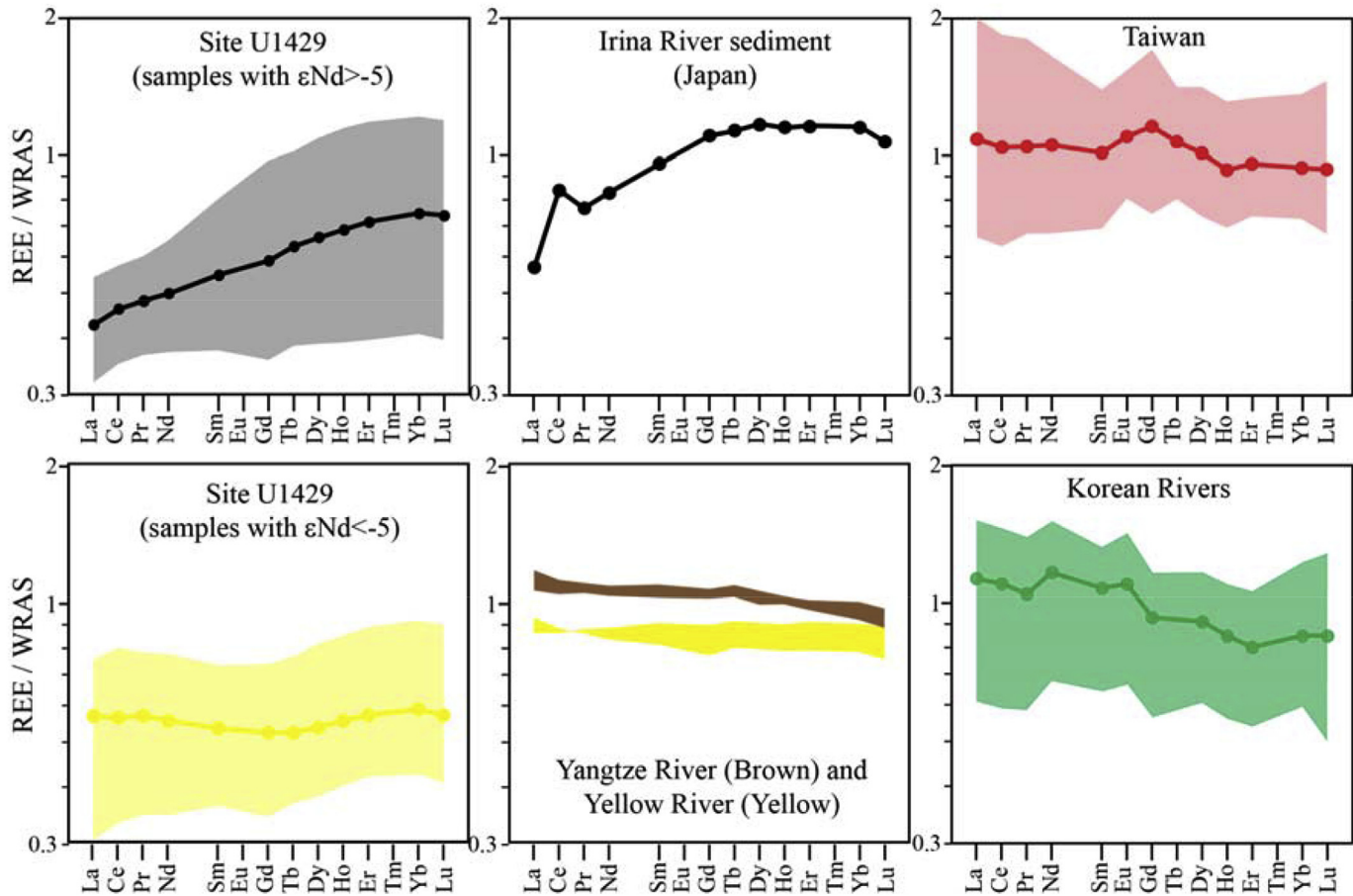


**Fig. 6.** WRAS-normalized REE patterns at Site U1429 and the main potential sources (Yellow and Yangtze rivers: Bayon et al., 2015; Korean rivers: Lee et al., 2003; Taiwan: Li et al., 2013; Irina river (Japan): this study. Colored envelopes denote the range of REE ratios. Lines and points indicate the average REE spectrum. Samples with radiogenic  $\epsilon_{\text{Nd}}$  are characterized by REE compositions similar to the Irina river while samples with  $\epsilon_{\text{Nd}}$  below  $-5$  exhibit a composition similar to the Chinese rivers. (For interpretation of the references to color in this figure legend, the reader is referred to the Web version of this article.)

**Table 3**

$\epsilon_{\text{Nd}}$  of the main potential sediment sources for Site U1429.

region	$\epsilon_{\text{Nd}}$ (min)	$\epsilon_{\text{Nd}}$ (max)	sample type	nombre of samples	references
Honchu Hokkaido	5,0	6,0	not precised	not given	Mahoney, 2005
Kyushu Shikoku	-6,0	4,0	not precised	not given	Mahoney, 2005
Southern Japanese volcanos	-6,0	-4,0	volcanos	>39	Ishizaka and Carlson, 1983; Chen et al., 1993; Mahoney, 2005
Kagoshima River	2,0	2,0	river sediment	1	this study
Taiwan	-15,0	-10,0	not precised	55	Chen et al., 1990; John et al., 1990
Yangtze River (mouth)	-13,0	-10,5	river sediment	18	Goldstein et al., 1984; Yang et al., 2007; Bayon et al., 2015
Yellow River (mouth)	-12,6	-10,9	river sediment	4	Goldstein et al., 1984; Yang et al., 2007; Bayon et al., 2015
Yellow River (all reaches)	-13,9	-9,6	river sediment	not given	Hu et al., 2012 and references therein
Korean rivers	-27,5	-13,1	river sediment	8	Lan et al., 1995
Korean cristaline massif	-33,6	-4,5	crystaline massif	58	Lan et al., 1995; Lee et al., 2003
North Tianshan	-6,6	-5,2	quaternary loess	>5	Liu et al., 1994 and references therein
SW Tarim Basin	-12,8	-9,1	quaternary loess	>11	Liu et al., 1994 and references therein
NE China	-9,6	-8,5	quaternary loess	>2	Liu et al., 1994 and references therein
Ordos Plateau	-21,0	-10,0	quaternary loess	not given	Chen et al., 2007; Sun et al., 2008; Hu et al., 2012
Central Loes Plateau	-12,0	-7,0	quaternary loess	not given	Chen et al., 2007; Sun et al., 2008; Hu et al., 2012
Nanjing	-12,2	-10,9	quaternary loess	not given	Liu et al., 1994 and references therein

increased inputs from the Loess Plateau and/or southern Japan (by comparison with glacial periods) in response to sea level changes as well as ITCZ migrations and associated changes in monsoon systems intensities. One can assume that, for MIS 6, sea-level variations, previously identified as a possible driver of orbital-scale variability in the  $\epsilon_{\text{Nd}}$  and REE, cannot explain the  $\epsilon_{\text{Nd}}$  variability alone. First, the sea-level change associated with MIS 6d (from  $\sim 80$

to  $\sim 50$  m) was relatively small ( $\sim 30$  m) in comparison to glacial/interglacial transitions ( $>100$  m; Waelbroeck et al., 2002; Grant et al., 2014). Second, the MIS6d sea-level change would have presumably acted as a sediment trap in such a shallow marine environment (e.g. Sweet and Blum, 2016). A period of increased river discharge can exceed the buffering effect of sea-level increases in the transfer of sediments from terrestrial sources to deep basin

sinks. Thus, we assume that enhanced rainfall occurred over the Yellow river watershed and/or southern Japanese regions during MIS 6d, and by extension that summer monsoon dominated conditions prevailed over East Asia. Such conditions are quite unexpected for the MIS 6, however, since northern hemisphere ice-sheets are known to have encouraged cold winter monsoon dominated conditions in East Asia (e.g. Wang et al., 2008). Exceptionally high abundances of thermal-humidiphilous mollusks (a species that is usually prevalent during interglacial periods) have been reported at ca. 170 ka in the Luochuan loess sequence (South Chinese Loess Plateau; Fig. 1), suggesting enhanced summer monsoon (Rousseau et al., 2009). The same conclusion can also be drawn from both Chinese (ca. 165–178 ka; Cheng et al., 2006, 2009; Wang et al., 2008) and Korean (ca. 168 ka; Jo et al., 2014) speleothem records. In addition, sedimentological results from the Xifeng loess sequence in the southern-central part of the Chinese Loess Plateau, about 150 km westward of Luochuan, suggest intervals with particular weak winter monsoon during the same interval (Guo et al., 2009). These results from the East Asian continent strongly support our hypothesis that increased rainfall, and thus summer monsoon dominated conditions, prevailed during the ~150–180 ka interval (MIS 6d).

At a larger scale, intensification of the North African summer monsoon and associated Nile discharges, in addition to unexpected wet conditions over the northern Mediterranean borderlands (Ayalon et al., 2002; Bard et al., 2002; Toucanne et al., 2015), also led to the deposition of the so-called sapropel S6 unit (ca. 165–178 ka, Ziegler et al., 2010; Rossignol-Strick, 1983). This linkage between East Asia and North Africa indicates that both regions may have been affected by synchronous, northward migration of the ITCZ. Thus, our data independently support the idea that the ITCZ was located over northern China and the southern Japan peninsula during MIS 6d. In agreement with recent work conducted on Korean speleothems (Jo et al., 2014), this reveals that our study area, as a mid-latitude temperate region and one of the northernmost parts of the East Asian monsoon sector, is significantly influenced by migrations of the mean latitudinal position of the ITCZ.

#### 4.6. Long-term fluctuations of ITCZ

A long-term change is observed in the  $\epsilon_{\text{Nd}}$  profile at Site U1429 (Fig. 2). The  $\epsilon_{\text{Nd}}$  data of the interglacial peaks show an increasing trend between MIS11 and MIS 5 (see Section 4.2). This trend is apparent for both the <2 µm and 30–63 µm size fractions, allowing us to rule out the dust contribution (see Section 4.1). Similarly, long-term climatic fluctuations are preserved in the general evolution of  $\delta^{18}\text{O}$  hydrological records in Chinese (i.e. Kesang, Sanbao and Hulu caves; Wang et al., 2008; Cheng et al., 2009, 2012, 2016) and Korean (Jo et al., 2014) speleothems, as well as southern Australia (Ayliiffe et al., 1998; Jo et al., 2014) (Fig. 2c and d), despite there being no discernible trend in the sea-level record (Waelbroeck et al., 2002; Grant et al., 2014) or oceanic circulation. The speleothem  $\delta^{18}\text{O}$  records, usually interpreted as a proxy for summer monsoon intensity, can also reflect precipitation sources (e.g., Pacific versus Indian Ocean; Clemens et al., 2010; Caley et al., 2014). It is difficult to link possible changes in precipitation sources to the changes observed in our  $\epsilon_{\text{Nd}}$  records, in particular for the Japanese peninsula and its small watersheds. Thus, the trend observed in both Asian-Australian speleothem  $\delta^{18}\text{O}$  (Fig. 2c and d) and in the Okinawa Trough  $\epsilon_{\text{Nd}}$  (Site U1429; Fig. 2a) is most likely related to rainfall and summer monsoon intensity. On this basis, we propose that the general evolution of the  $\epsilon_{\text{Nd}}$  record at Site U1429 reflects a gradual intensification of rainfall over East Asia (including the Yellow river watershed and the southern Japan) and/or an increase of the duration of the wet season (i.e., summer monsoon) in

the same areas. Thus, taken together with the speleothem  $\delta^{18}\text{O}$  records from East Asia and Australia, our data suggest a gradual, northward migration of the ITCZ during the successive interglacials from MIS11 to MIS5. It could also reveal, in the light of the hydrological seesaw pattern existing between East Asia and Australia (Jo et al., 2014), that the amplitude of the variations (i.e. latitudinal amplitudes) in the seasonal ITCZ could have gradually increased from MIS 11 to MIS 5. The assumptions detailed here require further testing. For example, producing high-resolution inorganic (radioactive and stable isotopes) and organic (e.g. long chain n-alkanes; Pelejero, 2003) geochemical investigations at Site U1429. Nonetheless, by providing the first long-term reconstruction of sediment discharge to the East China Sea during the Quaternary, this study improves our understanding of changes in East Asian monsoon dynamics and the attendant response of regional sediment routing systems over the last 400 kyr.

#### 5. Summary

The REE and Nd isotopic compositions of the clay (<2 µm) and non-cohesive silt (30–63 µm) detrital fractions of IODP Site U1429 sediments have been used to discuss patterns of the sediment transfer into the northern East China Sea (Danjo Basin, northern Okinawa Trough) over the last 400 kyr. Riverine inputs from the Yellow River and the Japanese archipelago have been identified as the main sediment sources. Their respective contributions at Site U1429 varied in phase with glacial-interglacial climate changes in response to both sea-level fluctuations, and the attendant reorganization of East Asian river mouth locations and ocean circulation on the East China Sea shelf, and latitudinal shifts of the ITCZ. Importantly, our results suggest a strengthening of the interglacial (summer) monsoon rainfall over the East Asian continent and Japan throughout the last 400 kyr, interpreted as a gradual northward migration of the ITCZ. Taken together with cave records, this study provides an indirect but valuable record of rainfall intensity over the East Asian continent and the Japanese Archipelago over the last four glacial-interglacial cycles and, by extension, new insights into the long-term evolution of the East Asian Monsoon.

#### Acknowledgments

Authors warmly thank N. Gayet and E. Pelleter for SEM analyses, S. Bermell for ArcGIS mapping, M.-L. Rouget for ICP-MS measurements, E. Ponzevera and Y. Germain for analyses with the Neptune MC-ICP-MS, and S. Chéron, J. Etoubleau, and A. Boissier for XRF measurements. Authors also express their special thanks to N. Freslon for help with ICP-MS measurements, S. Boswell for English improvements, and A. Bory and V. Bout-Roumazeilles for their support to the project. Authors finally thank all the scientific Expedition IODP 346 scientists, and Professor R. Tada (co-chief scientist) for his interest to this research. C.S. was partly supported by a Grant from the French government through Agence Nationale de la Recherche (ANR) under the 'Investissements d'Avenir' programme, reference ANR-10-LABX-19-0.

#### Appendix A. Supplementary data

Supplementary data related to this article can be found at <https://doi.org/10.1016/j.quascirev.2018.04.032>.

#### References

- An, Z., Tunghseng, L., Yanchou, L., Porter, S.C., Kukla, G.H.W.X., Xihao, W., Yingming, H., 1990. The long-term paleomonsoon variation recorded by the loess-paleosol sequence in central China. *Quat. Int.* 7, 91–95. [https://doi.org/10.1016/0169-555X\(90\)90007-2](https://doi.org/10.1016/0169-555X(90)90007-2)

- 10.1016/1040-6182(90)90042-3.
- An, Z., Porter, S.C., Kutzbach, J.E., Xihao, W., Suming, W., Xiaodong, L., Xiaoqiang, L., Weijian, Z., 2000. Asynchronous Holocene optimum of the East Asian monsoon. *Quat. Sci. Rev.* 19 (8), 743–762. [https://doi.org/10.1016/S0277-3791\(99\)00031-1](https://doi.org/10.1016/S0277-3791(99)00031-1).
- Ayalon, A., Bar-Matthews, M., Kaufman, A., 2002. Climatic conditions during marine oxygen isotope stage 6 in the eastern Mediterranean region from the isotopic composition of speleothems of Soreq Cave, Israel. *Geology* 30 (4), 303–306. [https://doi.org/10.1130/0091-7613\(2002\)030<0303:CCDMOI>2.2.CO;2](https://doi.org/10.1130/0091-7613(2002)030<0303:CCDMOI>2.2.CO;2).
- Ayliffe, L.K., Marianelli, P.C., Moriarty, K.C., Wells, R.T., McCulloch, M.T., Mortimer, G.E., Hellstrom, J.C., 1998. 500 ka precipitation record from southeastern Australia: evidence for interglacial relative aridity. *Geology* 26 (2), 147–150.
- Bard, E., Delaygue, G., Rostek, F., Antonioli, F., Silenzi, S., Schrag, D.P., 2002. Hydrological conditions over the western Mediterranean basin during the deposition of the cold Sapropel 6 (ca. 175 kyr BP). *Earth Planet. Sci. Lett.* 202 (2), 481–494. [https://doi.org/10.1016/S0012-821X\(02\)00788-4](https://doi.org/10.1016/S0012-821X(02)00788-4).
- Barrat, J.A., Keller, F., Amosse, J., Taylor, R.N., Nesbitt, R.W., Hirata, T., 1996. Determination of rare earth elements in sixteen silicate reference samples by ICP-MS after Tm addition and ion exchange separation. *Geostand. Geoanal. Res.* 20 (1), 133–139. <https://doi.org/10.1111/j.1751-908X.1996.tb00177.x>.
- Bayon, G., German, C.R., Boella, R.M., Milton, J.A., Taylor, R.N., Nesbitt, R.W., 2002. An improved method for extracting marine sediment fractions and its application to Sr and Nd isotopic analysis. *Chem. Geol.* 187 (3–4), 179–199. [https://doi.org/10.1016/S0009-2541\(01\)00416-8](https://doi.org/10.1016/S0009-2541(01)00416-8).
- Bayon, G., Barrat, J.A., Etoubleau, J., Benoit, M., Bollinger, C., Révillon, S., 2009. Determination of rare earth elements, Sc, Y, Zr, Ba, Hf and Th in geological samples by ICP-MS after Tm addition and alkaline fusion. *Geostand. Geoanal. Res.* 33 (1), 51–62. <https://doi.org/10.1111/j.1751-908X.2008.00880.x>.
- Bayon, G., Dennielou, B., Etoubleau, J., Ponzevera, E., Toucanne, S., Bermell, S., 2012. Intensifying weathering and land use in iron age central Africa. *Science* 335 (6073), 1219–1222. <https://doi.org/10.1126/science.1215400>.
- Bayon, G., Toucanne, S., Skonieczny, C., André, L., Bermell, S., Cheron, S., Dennielou, B., Etoubleau, J., Freslon, N., Gauchery, T., Germain, Y., Jorry, S.J., Ménot, G., Monin, G., Ponzevera, E., Rouget, M.-L., Tachikawa, K., Barrat, J.A., 2015. Rare earth elements and neodymium isotopes in world river sediments revisited. *Geochimica Cosmochim. Acta* 170, 17–38. <https://doi.org/10.1016/j.gca.2015.08.001>.
- Beardsley, R.C., Limeburner, R., Yu, H., Cannon, G.A., 1985. Discharge of the Changjiang (Yangtze River) into the East China Sea. *Cont. Shelf Res.* 4 (1–2), 57–76. [https://doi.org/10.1016/0278-4343\(85\)90022-6](https://doi.org/10.1016/0278-4343(85)90022-6).
- Caley, T., Roche, D.M., Renssen, H., 2014. Orbital Asian summer monsoon dynamics revealed using an isotope-enabled global climate model. *Nat. Commun.* 5, 5371. <https://doi.org/10.1038/ncomms6371>.
- Chang, Y.P., Chen, M.T., Yokoyama, Y., Matsuzaki, H., Thompson, W.G., Kao, S.J., Kawahata, H., 2009. Monsoon hydrography and productivity changes in the East China Sea during the past 100,000 years: Okinawa Trough evidence (MD012404). *Paleoceanography* 24 (3). <https://doi.org/10.1029/2007PA001577>.
- Chen, C.H., Jahn, B.M., Lee, T., Chen, C.H., Cornichet, J., 1990. Sm-Nd isotopic geochemistry of sediments from Taiwan and implications for the tectonic evolution of southeast China. *Chem. Geol.* 88 (3–4), 317–332. [https://doi.org/10.1016/0009-2541\(90\)90096-P](https://doi.org/10.1016/0009-2541(90)90096-P).
- Chen, C.H., DePaolo, D.J., Nakada, S., Shieh, Y.N., 1993. Relationship between eruption volume and neodymium isotopic composition at Unzen volcano. *Nature* 362 (6423), 831. <https://doi.org/10.1038/362831a0>.
- Chen, J., Wang, F., Meybeck, M., He, D., Xia, X., Zhang, L., 2005a. Spatial and temporal analysis of water chemistry records (1958–2000) in the Huanghe (Yellow River) basin. *Glob. Biogeochem. Cycles* 19 (3). <https://doi.org/10.1029/2004GB002325>.
- Chen, J., Li, G., Yang, J., Rao, W., Lu, H., Balsam, W., Sun, Y., Ji, J., 2007. Nd and Sr isotopic characteristics of Chinese deserts: implications for the provenances of Asian dust. *Geochimica Cosmochim. Acta* 71 (15), 3904–3914. <https://doi.org/10.1016/j.gca.2007.04.033>.
- Chen, Z., Wang, Z., Schneiderman, J., Taol, J., Cail, Y., 2005b. Holocene climate fluctuations in the Yangtze delta of eastern China and the Neolithic response. *Holocene* 15 (6), 915–924. <https://doi.org/10.1191/0959683605h1862r>.
- Cheng, H., Edwards, R.L., Wang, Y., Kong, X., Ming, Y., Kelly, M.J., Zhang, Liu, W., 2006. A penultimate glacial monsoon record from Hulu Cave and two-phase glacial terminations. *Geology* 34 (3), 217–220. <https://doi.org/10.1130/G22289.1>.
- Cheng, H., Edwards, R.L., Broecker, W.S., Denton, G.H., Kong, X., Wang, Y., Zhang, Y., Wang, X., 2009. Ice age terminations. *Science* 326 (5950), 248–252. <https://doi.org/10.1126/science.1177840>.
- Cheng, H., Sinha, A., Wang, X., Cruz, F.W., Edwards, R.L., 2012. The global paleomonsoon as seen through speleothem records from Asia and the Americas. *Clim. Dyn.* 39 (5), 1045–1062. <https://doi.org/10.1007/s00382-012-1363-7>.
- Cheng, H., Edwards, R.L., Sinha, A., Spötl, C., Yi, L., Chen, S., Kelly, M., Kathayat, G., Wang, X., Li, X., Kong, X., Wang, Y., Ning, Y., Zhang, H., 2016. The Asian monsoon over the past 640,000 years and ice age terminations. *Nature* 534 (7609), 640. <https://doi.org/10.1038/nature18591>.
- Clemens, S.C., Prell, W.L., Sun, Y., 2010. Orbital-scale timing and mechanisms driving Late Pleistocene Indo-Australian summer monsoons: reinterpreting cave speleothem  $\delta^{18}\text{O}$ . *Paleoceanography* 25 (4). <https://doi.org/10.1029/2010PA001926>.
- Diekmann, B., Hofmann, J., Henrich, R., Fütterer, D.K., Röhle, U., Wei, K.Y., 2008. Detrital sediment supply in the southern Okinawa Trough and its relation to sea-level and Kuroshio dynamics during the late Quaternary. *Mar. Geol.* 255 (1), 83–95. <https://doi.org/10.1016/j.margeo.2008.08.001>.
- Dou, Y., Yang, S., Liu, Z., Clift, P.D., Shi, X., Yu, H., Berne, S., 2010. Provenance discrimination of siliciclastic sediments in the middle Okinawa Trough since 30 ka: constraints from rare earth element compositions. *Mar. Geol.* 275 (1–4), 212–220. <https://doi.org/10.1016/j.margeo.2010.06.002>.
- Dou, Y., Yang, S., Liu, Z., Shi, X., Li, J., Yu, H., Berne, S., 2012. Sr–Nd isotopic constraints on terrigenous sediment provenances and Kuroshio Current variability in the Okinawa Trough during the late Quaternary. *Palaeogeogr. Palaeoclimatol. Palaeoecol.* 365, 38–47. <https://doi.org/10.1016/j.palaeo.2012.09.003>.
- Dykoski, C.A., Edwards, R.L., Cheng, H., Yuan, D., Cai, Y., Zhang, M., Lin, Y., Qing, J., An, J., Revenaugh, J., 2005. A high-resolution, absolute-dated Holocene and deglacial Asian monsoon record from Dongge Cave, China. *Earth Planet. Sci. Lett.* 233 (1–2), 71–86. <https://doi.org/10.1016/j.epsl.2005.01.036>.
- Expedition 346 Scientists, 2014. Asian Monsoon: Onset and Evolution of Millennial-scale Variability of Asian Monsoon and its Possible Relation with Himalaya and Tibetan Plateau Uplift. IODP Preliminary Report, vol. 346. [https://doi.org/10.2204/iodp.proc.346.2015\\_111p](https://doi.org/10.2204/iodp.proc.346.2015_111p).
- Feng, M., Mitsudera, H., Yoshikawa, Y., 2000. Structure and variability of the Kuroshio current in Tokara Strait. *J. Phys. Oceanogr.* 30 (9), 2257–2276. [https://doi.org/10.1175/1520-0485\(2000\)030](https://doi.org/10.1175/1520-0485(2000)030).
- Garçon, M., Chauvel, C., 2014. Where is basalt in river sediments, and why does it matter? *Earth Planet. Sci. Lett.* 407, 61–69. <https://doi.org/10.1016/j.epsl.2014.09.033>.
- Gao, Y., Arimoto, R., Duce, R.A., Zhang, X.Y., Zhang, G.Y., An, Z.S., Chen, L.Q., Zhou, M.Y., Gu, D.Y., 1997. Temporal and spatial distributions of dust and its deposition to the China Sea. *Tellus B Chem. Phys. Meteorol.* 49 (2), 172–189.
- Goldstein, S.L., O'Nions, R.K., Hamilton, P.J., 1984. A Sm–Nd isotopic study of atmospheric dusts and particulates from major river systems. *Earth Planet. Sci. Lett.* 70 (2), 221–236. [https://doi.org/10.1016/0012-821X\(84\)90007-4](https://doi.org/10.1016/0012-821X(84)90007-4).
- Grant, K.M., Rohling, E.J., Ramsey, C.B., Cheng, H., Edwards, R.L., Florindo, F., Hespel, D., Marra, F., Roberts, A.P., Tamisiea, M.E., Williams, F., 2014. Sea-level variability over five glacial cycles. *Nat. Commun.* 5, 5076. <https://doi.org/10.1038/ncomms6076>.
- Grouset, F.E., Parra, M., Bory, A., Martinez, P., Bertrand, P., Shimmield, G., Ellam, R.M., 1998. Saharan wind regimes traced by the Sr–Nd isotopic composition of subtropical Atlantic sediments: last glacial maximum vs today. *Quat. Sci. Rev.* 17 (4–5), 395–409. [https://doi.org/10.1016/S0277-3791\(97\)00048-6](https://doi.org/10.1016/S0277-3791(97)00048-6).
- Guo, Z.T., Berger, A., Yin, Q.Z., Qin, L., 2009. Strong asymmetry of hemispheric climates during MIS-13 inferred from correlating China loess and Antarctica ice records. *Clim. Past* 5 (1), 21–31. <https://doi.org/10.5194/cp-5-21-2009>.
- Hu, B., Li, G., Li, J., Bi, J., Zhao, J., Bu, R., 2012. Provenance and climate change inferred from Sr–Nd–Pb isotopes of late Quaternary sediments in the Huanghe (Yellow River) Delta, China. *Quat. Res.* 78 (3), 561–571. <https://doi.org/10.1016/j.yqres.2012.07.005>.
- Huh, C.A., Su, C.C., Wang, C.H., Lee, S.Y., Lin, I.T., 2006. Sedimentation in the southern Okinawa Trough—rates, turbidites and a sediment budget. *Mar. Geol.* 231 (1–4), 129–139. <https://doi.org/10.1016/j.margeo.2006.05.009>.
- Ishizaka, K., Carlson, R.W., 1983. Nd–Sr systematics of the Setouchi volcanic rocks, southwest Japan: a clue to the origin of orogenic andesite. *Earth Planet. Sci. Lett.* 64 (3), 327–340. [https://doi.org/10.1016/0012-821X\(83\)90094-8](https://doi.org/10.1016/0012-821X(83)90094-8).
- Jacobsen, S.B., Wasserburg, G.J., 1980. Sm–Nd isotopic evolution of chondrites. *Earth Planet. Sci. Lett.* 50 (1), 139–155. [https://doi.org/10.1016/0012-821X\(80\)90125-9](https://doi.org/10.1016/0012-821X(80)90125-9).
- Jian, Z., Wang, P., Saito, Y., Wang, J., Pflaumann, U., Oba, T., Cheng, X., 2000. Holocene variability of the Kuroshio current in the Okinawa Trough, northwestern Pacific ocean. *Earth Planet. Sci. Lett.* 184 (1), 305–319. [https://doi.org/10.1016/S0012-821X\(00\)00321-6](https://doi.org/10.1016/S0012-821X(00)00321-6).
- Jo, K.N., Woo, K.S., Yi, S., Yang, D.Y., Lim, H.S., Wang, Y., Cheng, H., Edwards, R.L., 2014. Mid-latitude interhemispheric hydrologic seesaw over the past 550,000 years. *Nature* 508 (7496), 378. <https://doi.org/10.1038/nature13076>.
- John, B.M., Zhou, X.H., Li, J.L., 1990. Formation and tectonic evolution of southeastern China and Taiwan: isotopic and geochemical constraints. *Tectonophysics* 183 (1–4), 145–160. [https://doi.org/10.1016/0040-1951\(90\)90413-3](https://doi.org/10.1016/0040-1951(90)90413-3).
- Kapp, P., Pelletier, J.D., Rohrmann, A., Heermance, R., Russell, J., Ding, L., 2011. Wind erosion in the Qaidam basin, central Asia: implications for tectonics, paleoclimate, and the source of the Loess Plateau. *GSA Today* 21 (4/5), 4–10. <https://doi.org/10.1130/GSATG99A.1>.
- Kao, S.J., Wu, C.R., Hsin, Y.C., Dai, M., 2006. Effects of sea level change on the upstream Kuroshio current through the Okinawa Trough. *Geophys. Res. Lett.* 33 (16). <https://doi.org/10.1029/2006GL026822>.
- Kubota, Y., Kimoto, K., Tada, R., Oda, H., Yokoyama, Y., Matsuzaki, H., 2010. Variations of East Asian summer monsoon since the last deglaciation based on Mg/Ca and oxygen isotope of planktic foraminifera in the northern East China Sea. *Paleoceanography* 25 (4). <https://doi.org/10.1029/2009PA001891>.
- Lan, C.Y., Lee, T., Zhou, X.H., Kwon, S.T., 1995. Nd isotopic study of Precambrian basement of South Korea: evidence for Early Archean crust? *Geology* 23 (3), 249–252. [https://doi.org/10.1130/0091-7613\(1995\)023](https://doi.org/10.1130/0091-7613(1995)023).
- Laskar, J., Robutel, P., Joutel, F., Gastineau, M., Correia, A.C.M., Levrard, B., 2004. A long-term numerical solution for the insolation quantities of the Earth. *Astron. Astrophys.* 428 (1), 261–285. <https://doi.org/10.1051/0004-6361:20041335>.
- Lee, H.J., Chao, S.Y., 2003. A climatological description of circulation in and around the East China Sea. *Deep Sea Res. Part II Top. Stud. Oceanogr.* 50 (6–7), 1065–1084. [https://doi.org/10.1016/S0967-0645\(03\)00010-9](https://doi.org/10.1016/S0967-0645(03)00010-9).
- Lee, S.R., Cho, M., Hwang, J.H., Lee, B.J., Kim, Y.B., Kim, J.C., 2003. Crustal evolution of

- the Gyeonggi massif, South Korea: Nd isotopic evidence and implications for continental growths of East Asia. *Precambrian Res.* 121 (1–2), 25–34. <https://doi.org/10.1016/j.precamres.2002.00196-1>.
- Li, C.S., Shi, X.F., Kao, S.J., Liu, Y.G., Lyu, H.H., Zou, J.J., Liu, S.-F., Qiao, S.Q., 2013. Rare earth elements in fine-grained sediments of major rivers from the high-standing island of Taiwan. *J. Asian Earth Sci.* 69, 39–47. <https://doi.org/10.1016/j.jseas.2013.03.001>.
- Li, T., Xu, Z., Lim, D., Chang, F., Wan, S., Jung, H., Choi, J., 2015. Sr–Nd isotopic constraints on detrital sediment provenance and paleoenvironmental change in the northern Okinawa Trough during the late Quaternary. *Palaeogeogr. Palaeoclimatol. Palaeoecol.* 430, 74–84. <https://doi.org/10.1016/j.palaeo.2015.04.017>.
- Lin, A., Yang, Z., Sun, Z., Yang, T., 2001. How and when did the Yellow River develop its square bend? *Geology* 29 (10), 951–954. <https://doi.org/10.1130/0091-7613.127.10-25>.
- Liu, C.Q., Masuda, A., Okada, A., Yabuki, S., Fan, Z.L., 1994. Isotope geochemistry of Quaternary deposits from the arid lands in northern China. *Earth Planet. Sci. Lett.* 127 (1–4), 25–38. [https://doi.org/10.1016/0012-821X\(94\)90195-3](https://doi.org/10.1016/0012-821X(94)90195-3).
- Liu, Z., Treteaux, A., Clemens, S.C., Colin, C., Wang, P., Huang, B., Boulay, S., 2003. Clay mineral assemblages in the northern South China Sea: implications for East Asian monsoon evolution over the past 2 million years. *Mar. Geol.* 201 (1), 133–146. [https://doi.org/10.1016/S0025-3227\(03\)00213-5](https://doi.org/10.1016/S0025-3227(03)00213-5).
- Liu, J.P., Xu, K.H., Li, A.E.A., Milliman, J.D., Velozi, D.M., Xiao, S.B., Yang, Z.S., 2007. Flux and fate of Yangtze river sediment delivered to the East China sea. *Geomorphology* 85 (3–4), 208–224. <https://doi.org/10.1016/j.geomorph.2006.03.023>.
- Lugmair, G.W., Shimamura, T., Lewis, R.S., Anders, E., 1983. Samarium-146 in the early solar system: evidence from neodymium in the Allende meteorite. *science* 222 (4627), 1015–1018. <https://doi.org/10.1126/science.222.4627.1015>.
- Mahoney, J.B., 2005. Nd and Sr isotopic signatures of fine-grained clastic sediments: a case study of western Pacific marginal basins. *Sediment. Geol.* 182 (1), 183–199. <https://doi.org/10.1016/j.sedgeo.2005.07.009>.
- Meng, X., Liu, L., Wang, X.T., Balsam, W., Chen, J., Ji, J., 2018. Mineralogical evidence of reduced East Asian summer monsoon rainfall on the Chinese loess plateau during the early Pleistocene interglacials. *Earth Planet. Sci. Lett.* 486, 61–69. <https://doi.org/10.1016/j.epsl.2017.12.048>.
- Meyer, I., Davies, G.R., Stuut, J.B.W., 2011. Grain size control on Sr–Nd isotope provenance studies and impact on paleoclimate reconstructions: an example from deep-sea sediments offshore NW Africa. *Geochem. Geophys. Geosystems* 12 (3). <https://doi.org/10.1029/2010GC003355>.
- Milliman, J.D., Yun-Shan, Q., Mei-e, R., Saito, Y., 1987. Man's influence on the erosion and transport of sediment by Asian rivers: the Yellow River (Huanghe) example. *J. Geol.* 95 (6), 751–762. <https://doi.org/10.1086/629175>.
- Milliman, J.D., Syvitski, J.P., 1992. Geomorphic/tectonic control of sediment discharge to the ocean: the importance of small mountainous rivers. *J. Geol.* 100 (5), 525–544. <https://doi.org/10.1086/629066>.
- Nagashima, K., Tada, R., Tani, A., Sun, Y., Isozaki, Y., Toyoda, S., Hasegawa, H., 2011. Millennial-scale oscillations of the westerly jet path during the last glacial period. *J. Asian Earth Sci.* 40 (6), 1214–1220. <https://doi.org/10.1016/j.jseas.2010.08.010>.
- Oiwane, H., Tonai, S., Kiyokawa, S., Nakamura, Y., Suganuma, Y., Tokuyama, H., 2011. Geomorphological development of the Goto submarine Canyon, northeastern East China sea. *Mar. Geol.* 288 (1–4), 49–60. <https://doi.org/10.1016/j.margeo.2011.06.013>.
- Pelejero, C., 2003. Terrigenous n-alkane input in the South China Sea: high-resolution records and surface sediments. *Chem. Geol.* 200 (1–2), 89–103. [https://doi.org/10.1016/S0009-2541\(03\)00164-5](https://doi.org/10.1016/S0009-2541(03)00164-5).
- Porter, S.C., Hallet, B., Wu, X., An, Z., 2001. Dependence of near-surface magnetic susceptibility on dust accumulation rate and precipitation on the Chinese Loess Plateau. *Quat. Res.* 55 (3), 271–283. <https://doi.org/10.1006/qres.2001.2224>.
- Pullen, A., Kapp, P., McCallister, A.T., Chang, H., Gehrels, G.E., Garzione, C.N., Heerman, R.V., Ding, L., 2011. Qaidam Basin and northern Tibetan Plateau as dust sources for the Chinese Loess Plateau and paleoclimatic implications. *Geology* 39 (11), 1031–1034. <https://doi.org/10.1130/G32296.1>.
- Railsback, L.B., Gibbard, P.L., Head, M.J., Voarintsoa, N.R.G., Toucanne, S., 2015. An optimized scheme of lettered marine isotope substages for the last 1.0 million years, and the climatostratigraphic nature of isotope stages and substages. *Quat. Sci. Rev.* 111, 94–106. <https://doi.org/10.1016/j.quascirev.2015.01.012>.
- Rossignol-Strick, M., 1983. African monsoons, an immediate climate response to orbital insolation. *Nature* 304 (5921), 46. <https://doi.org/10.1038/304046a0>.
- Rousseau, D.D., Wu, N., Pei, Y., Li, F., 2009. Three exceptionally strong East-Asian summer monsoon events during glacial times in the past 470 kyr. *Clim. Past* 5 (2), 157–169. <https://doi.org/10.5194/cp-5-157-2009>.
- Sagawa, T., Nagashashi, Y., Satoguchi, Y., Holbourn, A., Itaki, T., Gallagher, S.J., Saaverdra-Pellitero, M., Ikheara, K., Irino, T., Tada, R., 2018. Integrated tephrostratigraphy and stable isotope stratigraphy in the Japan sea and east China sea using IODP sites U1426, U1427, and U1429, expedition 346 asian monsoon. *Prog. Earth Planet. Sci.* 5 (1), 18. <https://doi.org/10.1186/s40645-018-0168-7>.
- Saito, Y., Yang, Z., Hori, K., 2001. The Huanghe (Yellow River) and Changjiang (Yangtze River) deltas: a review on their characteristics, evolution and sediment discharge during the Holocene. *Geomorphology* 41 (2–3), 219–231. [https://doi.org/10.1016/S0169-555X\(01\)00018-0](https://doi.org/10.1016/S0169-555X(01)00018-0).
- Sun, Y., Oppo, D.W., Xiang, R., Liu, W., Gao, S., 2005. Last deglaciation in the Okinawa Trough: subtropical northwest pacific link to northern hemisphere and tropical climate. *Paleoceanography* 20 (4). <https://doi.org/10.1029/2004PA001061>.
- Sun, Y., Clemens, S.C., An, Z., Yu, Z., 2006. Astronomical timescale and palaeoclimatic implication of stacked 3.6-Myr monsoon records from the Chinese Loess Plateau. *Quat. Sci. Rev.* 25 (1–2), 33–48. <https://doi.org/10.1016/j.quascirev.2005.07.005>.
- Sun, Y., Tada, R., Chen, J., Liu, Q., Toyoda, S., Tani, A., Ji, J., Isozaki, Y., 2008. Tracing the provenance of fine-grained dust deposited on the central Chinese Loess Plateau. *Geophys. Res. Lett.* 35 (1). <https://doi.org/10.1029/2007GL031672>.
- Sweet, M.L., Blum, M.D., 2016. Connections between fluvial to shallow marine environments and submarine canyons: implications for sediment transfer to deep water. *J. Sediment. Res.* 86 (10), 1147–1162. <https://doi.org/10.2110/jsr.2016.64>.
- Tanaka, T., Togashi, S., Kamioka, H., Amakawa, H., Kagami, H., Hamamoto, T., Yuhara, M., Orihashi, Y., Yoneda, S., Shimizu, H., Kunimaru, T., Takahashi, K., Yanagi, T., Nakano, T., Fujimaki, H., Shinjo, R., Asahara, Y., Tanimizu, M., Dragusin, C., 2000. JNDI-1: a neodymium isotopic reference in consistency with LaJolla neodymium. *Chem. Geol.* 168 (3–4), 279–281. [https://doi.org/10.1016/S0009-2541\(00\)00198-4](https://doi.org/10.1016/S0009-2541(00)00198-4).
- Toucanne, S., Minto'o, C.M.A., Fontanier, C., Bassetti, M.A., Jorry, S.J., Jouet, G., 2015. Tracking rainfall in the northern Mediterranean borderlands during sapropel deposition. *Quat. Sci. Rev.* 129, 178–195. <https://doi.org/10.1016/j.quascirev.2015.10.016>.
- Ujiie, H., Tanaka, Y., Ono, T., 1991. Late Quaternary paleoceanographic record from the middle Ryukyu Trench slope, northwest Pacific. *Mar. Micropaleontol.* 18 (1–2), 115–128. [https://doi.org/10.1016/0377-8398\(91\)90008-T](https://doi.org/10.1016/0377-8398(91)90008-T).
- Ujiie, H., Ujiie, Y., 1999. Late quaternary course changes of the Kuroshio current in the ryukyu arc region, northwestern pacific ocean. *Mar. Micropaleontol.* 37 (1), 23–40. [https://doi.org/10.1016/S0377-8398\(99\)00010-9](https://doi.org/10.1016/S0377-8398(99)00010-9).
- Ujiie, Y., Ujiie, H., Taira, A., Nakamura, T., Oguri, K., 2003. Spatial and temporal variability of surface water in the Kuroshio source region, Pacific Ocean, over the past 21,000 years: evidence from planktonic foraminifera. *Mar. Micropaleontol.* 49 (4), 335–364. [https://doi.org/10.1016/S0377-8398\(03\)00062-8](https://doi.org/10.1016/S0377-8398(03)00062-8).
- Waelbroeck, C., Labeyrie, L., Michel, E., Duplessy, J.C., McManus, J.F., Lambeck, K., Balbon, E., Labracherie, M., 2002. Sea-level and deep water temperature changes derived from benthic foraminifera isotopic records. *Quat. Sci. Rev.* 21 (1–3), 295–305. [https://doi.org/10.1016/S0277-3791\(01\)00101-9](https://doi.org/10.1016/S0277-3791(01)00101-9).
- Wang, L., Sarnthein, M., Erlenkeuser, H., Grimalt, J., Grootes, P., Heilig, S., Ivanova, E., Kienast, M., Pelejero, C., Pflaumann, U., 1999. East Asian monsoon climate during the late Pleistocene: high-resolution sediment records from the south China sea. *Mar. Geol.* 156 (1), 245–284. [https://doi.org/10.1016/S0025-3227\(98\)00182-0](https://doi.org/10.1016/S0025-3227(98)00182-0).
- Wang, Y.J., Cheng, H., Edwards, R.L., An, Z.S., Wu, J.Y., Shen, C.C., Dorale, J.A., 2001. A high-resolution absolute-dated late Pleistocene monsoon record from Hulu Cave, China. *science* 294 (5550), 2345–2348. <https://doi.org/10.1126/science.1064618>.
- Wang, Y., Cheng, H., Edwards, R.L., Kong, X., Shao, X., Chen, S., Wu, J., Jiang, X., Wang, X., An, Z., 2008. Millennial-and orbital-scale changes in the East Asian monsoon over the past 224,000 years. *Nature* 451 (7182), 1090. <https://doi.org/10.1038/nature06692>.
- Xiao, J.L., An, Z.S., Liu, T.S., Inouchi, Y., Kumai, H., Yoshikawa, S., Kondo, Y., 1999. East Asian monsoon variation during the last 130,000 years: evidence from the Loess Plateau of central China and lake biwa of Japan. *Quat. Sci. Rev.* 18 (1), 147–157. [https://doi.org/10.1016/S0277-3791\(97\)00097-8](https://doi.org/10.1016/S0277-3791(97)00097-8).
- Xiao, J., Xu, Q., Nakamura, T., Yang, X., Liang, W., Inouchi, Y., 2004. Holocene vegetation variation in the Dihai Lake region of north-central China: a direct indication of the Asian monsoon climatic history. *Quat. Sci. Rev.* 23 (14–15), 1669–1679. <https://doi.org/10.1016/j.quascirev.2004.01.005>.
- Xiao, S., Li, A., Liu, J.P., Chen, M., Xie, Q., Jiang, F., Li, T., Xiang, R., Chen, Z., 2006. Coherence between solar activity and the East Asian winter monsoon variability in the past 8000 years from Yangtze River-derived mud in the East China Sea. *Palaeogeogr. Palaeoclimatol. Palaeoecol.* 237 (2–4), 293–304. <https://doi.org/10.1016/j.palaeo.2005.12.003>.
- Xu, D.Y., Kang, X.W., Zhuang, D.F., Pan, J.J., 2010. Multi-scale quantitative assessment of the relative roles of climate change and human activities in desertification—A case study of the Ordos Plateau, China. *J. Arid Environ.* 74 (4), 498–507. <https://doi.org/10.1016/j.jaridenv.2009.09.030>.
- Xu, Z., Li, T., Chang, F., Wan, S., Choi, J., Lim, D., 2014. Clay-sized sediment provenance change in the northern Okinawa Trough since 22kyrBP and its paleoenvironmental implication. *Palaeogeogr. Palaeoclimatol. Palaeoecol.* 399, 236–245. <https://doi.org/10.1016/j.palaeo.2014.01.016>.
- Yang, S.Y., Jung, H.S., Choi, M.S., Li, C.X., 2002. The rare earth element compositions of the Changjiang (Yangtze) and Huanghe (Yellow) river sediments. *Earth Planet. Sci. Lett.* 201 (2), 407–419. [https://doi.org/10.1016/S0012-821X\(02\)00715-X](https://doi.org/10.1016/S0012-821X(02)00715-X).
- Yang, S., Jiang, S., Ling, H., Xia, X., Sun, M., Wang, D., 2007. Sr–Nd isotopic compositions of the Changjiang sediments: implications for tracing sediment sources. *Sci. China Ser. D Earth Sci.* 50 (10), 1556–1565. <https://doi.org/10.1007/s11430-007-0052-6>.
- Yang, S., Ding, Z., 2008. Advance–retreat history of the East-Asian summer monsoon belt over northern China during the last two glacial–interglacial cycles. *Earth Planet. Sci. Lett.* 274 (3–4), 499–510. <https://doi.org/10.1016/j.epsl.2008.08.001>.
- Yi, S., Saito, Y., Zhao, Q., Wang, P., 2003. Vegetation and climate changes in the Changjiang (Yangtze River) Delta, China, during the past 13,000 years inferred from pollen records. *Quat. Sci. Rev.* 22 (14), 1501–1519. [https://doi.org/10.1016/S0277-3791\(03\)00080-5](https://doi.org/10.1016/S0277-3791(03)00080-5).
- Yi, S., Saito, Y., 2004. Latest Pleistocene climate variation of the East Asian monsoon from pollen records of two East China regions. *Quat. Int.* 121 (1), 75–87. <https://doi.org/10.1016/j.quaint.2004.02.017>.

- Yu, H., Liu, Z., Berné, S., Jia, G., Xiong, Y., Dickens, G.R., Wei, G., Shi, X., Liu, J.P., Chen, F., 2009. Variations in temperature and salinity of the surface water above the middle Okinawa Trough during the past 37 kyr. *Palaeogeogr. Palaeoclimatol. Palaeoecol.* 281 (1–2), 154–164. <https://doi.org/10.1016/j.palaeo.2009.08.002>.
- Yuan, D., Cheng, H., Edwards, R.L., Dykoski, C.A., Kelly, M.J., Zhang, M., Qing, J., Lin, Y., Wang, Y., Wu, J., Dorale, J.A., An, Z., Cai, Y., 2004. Timing, duration, and transitions of the last interglacial Asian monsoon. *Science* 304 (5670), 575–578. <https://doi.org/10.1126/science.1091220>.
- Zhao, D., Wan, S., Toucanne, S., Clift, P.D., Tada, R., Révillon, S., Kubota, Y., Zheng, X., Yu, Z., Huang, J., Jiang, H., Xu, Z., Shi, X., Li, A., 2017. Distinct control mechanism of fine-grained sediments from Yellow River and Kyushu supply in the northern Okinawa Trough since the last glacial. *Geochem. Geophys. Geosystems*. <https://doi.org/10.1002/2016GC006764>.
- Zhao, D., Wan, S., Clift, P.D., Tada, R., Huang, J., Yin, X., Liao, X., Shen, X., Shi, X., Li, A., 2018. Provenance, sea-level and monsoon climate controls on silicate weathering of Yellow River sediment in the northern Okinawa Trough during late last glaciation. *Palaeogeogr. Palaeoclimatol. Palaeoecol.* 490, 227–239. <https://doi.org/10.1016/j.palaeo.2017.11.002>.
- Zhisheng, A., Kutzbach, J.E., Prell, W.L., Porter, S.C., 2001. Evolution of Asian monsoons and phased uplift of the Himalaya–Tibetan plateau since Late Miocene times. *Nature* 411 (6833), 62. <https://doi.org/10.1038/35075035>.
- Ziegler, M., Tuenter, E., Lourens, L.J., 2010. The precession phase of the boreal summer monsoon as viewed from the eastern Mediterranean (ODP Site 968). *Quat. Sci. Rev.* 29 (11), 1481–1490. <https://doi.org/10.1016/j.quascirev.2010.03.011>.